ACS OMEGA

http://pubs.acs.org/journal/acsodf

Article

Synthesis, Biological Evaluation, 2D-QSAR, and Molecular Simulation Studies of Dihydropyrimidinone Derivatives as Alkaline Phosphatase Inhibitors

Reem Altaf,* Humaira Nadeem, Muhammad Nasir Iqbal, Umair Ilyas, Zaman Ashraf, Muhammad Imran, and Syed Aun Muhammad*

Cite This: *ACS Omega* 2022, 7, 7139−7154

Read Online

ACCESS | Metrics & More | Article Recommendations

ABSTRACT: The presence of alkaline phosphatases has been observed in several species and has been known to play a crucial role in various biological functions. Higher expressions of alkaline phosphatase have been found in several multifactorial disorders and cancer patients, which has led it to be an interesting target for drug discovery. A strong structural similarity exists between intestinal alkaline phosphatases (IAPs) and tissue-nonspecific alkaline phosphatases (TNAPs), which has led to the discovery of only a few selective inhibitors. Therefore, a series of 22 derivatives of 6-(chloromethyl)-4-(4-hydroxyphenyl)-2-oxo-1,2,3,4-tetrahydropyrimidine-5-carboxylate (**1**) and ethyl 6-(chloromethyl)-4-(2-hydroxyphenyl)-2-oxo-1,2,3,4-tetrahydropyrimidine-5-carboxylate (**2**) were synthesized to evaluate the anticancer potential of these compounds against breast cancer. The compounds were characterized through spectral and elemental analyses. The inhibitory effect of dihydropyrimidinone derivatives on alkaline phosphatases was evaluated using the calf alkaline phosphatase assay. The antioxidant activity of these compounds was performed to study the radical scavenging effect. *In silico* molecular docking and molecular dynamic simulations were performed to elucidate the binding mode of active compounds. Moreover, the two-dimensional qualitative-structure−activity relationship (2D-QSAR) was performed to study the structural requirements for enzyme inhibition. The calf alkaline phosphatase inhibitory assay revealed significant inhibition of the enzyme by compound **4d** with IC_{50} 1.27 μM at 0.1 mM concentration as compared to standard KH_2PO_4 having IC_{50} 2.80 μM. The compounds **4f**, **4e**, and **4i** also showed very good inhibition with IC_{50} values of 2.502, 2.943, and 2.132 μM, respectively, at the same concentration. The antioxidant assay revealed efficient radical scavenging activity of compounds **4f**, **4e**, and **4g** at 100 μg/mL with IC_{50} values of 0.48, 0.61, and 0.75 μg/mL, respectively. The molecular docking and simulation studies revealed efficient binding of active compounds in the active binding site of the target enzyme. The final QSAR equation revealed good predictivity and statistical validation having R^2 = 0.958 and Q^2 = 0.903, respectively, for the generated model. The compound **4d** showed the highest inhibitory activity with stable binding modes acting as a future lead for identifying alkaline phosphatase inhibitors. The molecular simulations suggested the stable binding of this compound, and the QSAR studies revealed the importance of autocorrelated descriptors in the inhibition of alkaline phosphatase. The investigated compounds may serve as potential pharmacophores for potent and selective alkaline phosphatase inhibitors. We intend to further investigate the biological activities of these compounds as alkaline phosphatase inhibitors.

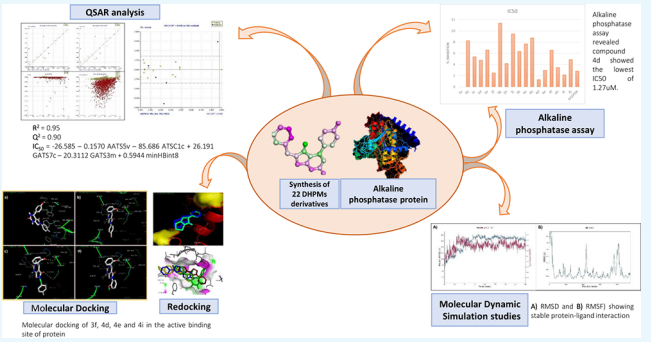

INTRODUCTION

The family of ectonucleotidase enzymes consists of an important family of enzymes, namely, alkaline phosphatases (APs), involved in catalyzing various transphosphorylation reactions.[1] Alkaline phosphatases are metallo-enzymes having five cysteine residues, one zinc atom, and one magnesium atom that are responsible for their catalytic activity. Alkaline phosphatases, as the name suggests, work in an alkaline medium and dephosphorylate monoesters to ensure normal functioning of cells such as protein phosphorylation, apoptosis, and cellular growth. Several organisms have been found having APs ranging from bacteria to men. In humans, four types of AP isoenzymes have been found, out of which three are considered tissue-specific, while the fourth one is tissue-nonspecific AP (TNAP).

Received: December 3, 2021
Accepted: February 8, 2022
Published: February 18, 2022

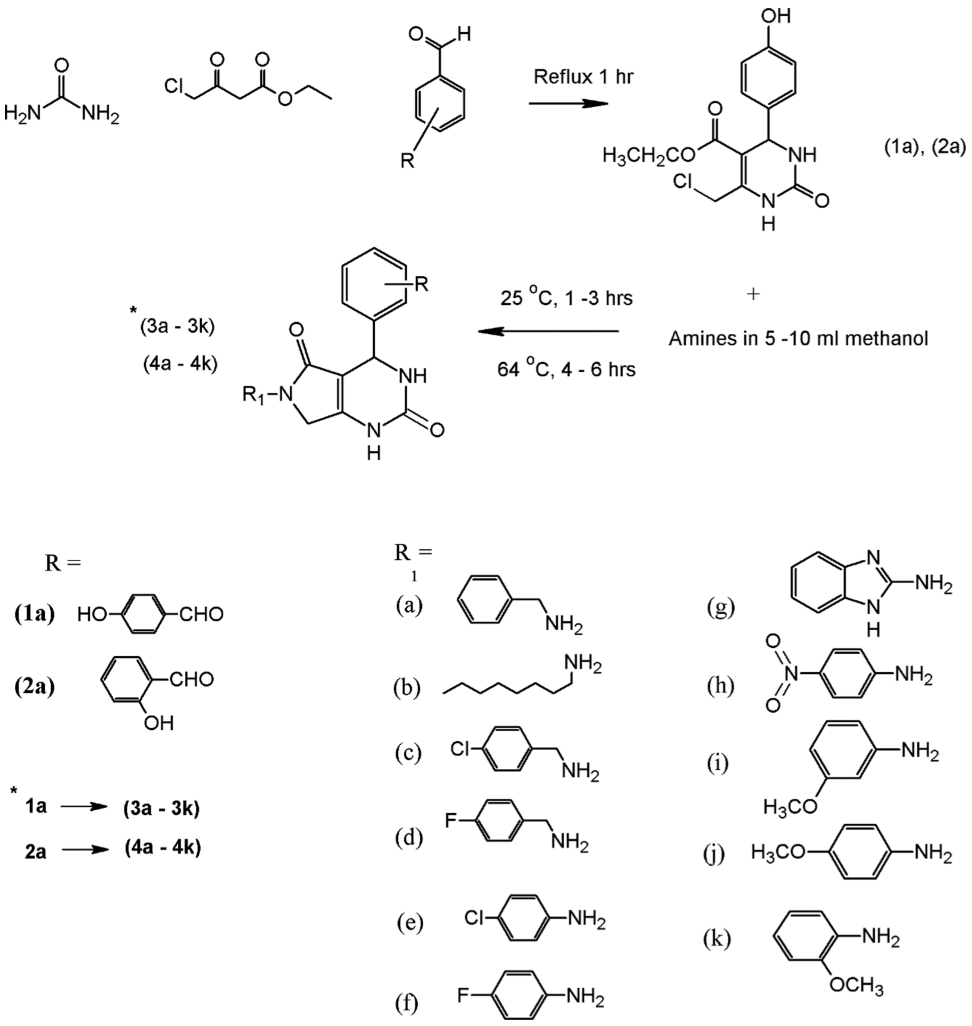

Figure 1. General scheme for the synthesis of dihydropyrimidinone derivatives.

The tissue-specific isoenzymes include placental AP (PLAP), intestinal AP (IAP), and germ cell AP (GCAP).[2] The tissue-nonspecific isoenzymes are found throughout the body, with the liver, kidney, and bone having the maximum expression maintaining an optimum pyrophosphate level in bone tissues by performing inorganic pyrophosphate (PPi) hydrolysis. The intestinal APs have been found to act as lipopolysaccharide (LPS)-detoxifying enzymes due to their presence in the epithelial linings of the intestine. The overexpression of intestinal APs has been found in various types of disorders such as atheroscelorosis, sepsis, arthritis, multiple sclerosis, and bowel diseases.[3] Moreover, the high level of TNAPs and IAPs has also been associated with several types of cancers such as esophageal, breast, prostrate, intestinal, ovarian, and liver cancers.[4] The higher expression of AP in cancer patients suggests metastasis to the liver and bone. Elevated levels of IAPs have been found in hepatocellular carcinomas,[5] and higher TNAP plasma levels have been found to be associated with osteocarcinomas, breast cancer, and osteoblastic bone metastasis. A strong structural similarity exists between IAPs and TNAPs, which has led to the discovery of only a few selective inhibitors such as theophylline, L-phenylalanine, levamisole, and imidazole.[6] Due to the increased plasma levels of APs in cancer patients as well as in several multifactorial disorders, they act as interesting molecular targets for drug discovery.

The structural similarity of pyrimidinones to the bioactive natural products and because of the presence of pyrimidine as a basic nucleus in DNA and RNA, these compounds have been associated with various biological activities.[7] The dihydropyrimidinones (DHPMs) have shown several important biological activities such as antibacterial, calcium channel blocking, antihypertensive, anti-inflammatory, and cytotoxic activities.[8] This significant nature of dihydropyrimidinones has led to the synthesis of a series of amine-containing dihydropyrimidinones and the evaluation of their biological activities. The *in vitro* calf intestinal alkaline phosphatase assay was performed to evaluate the inhibitory effect. The *in silico* molecular docking and molecular dynamic (MD) simulations were performed to analyze the binding mode of these compounds with the target protein. The two-dimensional qualitative-structure−activity relationship (2D-QSAR) studies were also conducted to evaluate the structural requirements of these compounds for AP inhibition.

RESULTS

Chemistry. Figure 1 was used to synthesize 22 derivatives of dihydropyrimidinones. 6-Chloromethyl-DHPMs were obtained under a neat reaction of urea, substituted benzaldehyde, and 4-chloroacetoacetate for 1 h under reflux. These compounds were obtained in 72−85% yield after precipitation from water. The

https://doi.org/10.1021/acsomega.1c06833
ACS Omega 2022, 7, 7139−7154

resulting compounds were treated with 5−10 mL of methanol benzylamine. The mixture was first refluxed at 25 °C for 1−3 h and then at 64 °C for 5−6 h. The reaction was cooled to ambient temperature and the solid product was filtered and washed with cold methanol to obtain the sample of desired pyrrolopyrimidines. The crystals obtained were then recrystallized in ethanol. The synthesized compounds were purified by column chromatography using petroleum ether/ethyl acetate at a ratio of 4:1 as the eluent. The spectral analysis of these compounds was done using Fourier transform infrared (FTIR), ^{1}H NMR, ^{13}C NMR, and elemental analyses. In FTIR, the presence of the −NH group at 3350 and the aide group at 1680 confirmed the synthesis of compounds (**3a** to **4k**). The ^{1}H NMR showed a singlet at 9.16 ppm, confirming the presence of the −NH group; a singlet of the methylene group at 4.10 and 4.33 ppm and a singlet of the CH group at 5.10 ppm were also observed, indicating the formation of products. Mass spectral analysis of **4f** was done using ionization mode electrospray ionization mass spectrometry (EIMS) with the JEOL 600H-1 instrument. Molecular ion peaks were not observed in the spectrum due to expulsion of the CO fragment from the molecular ion. A peak at m/z 311 was observed as a result of this fragmentation. Further expulsion of the C5 H5 moiety from the molecular ion resulted in the base peak at m/z 274. Removal of the *p*-fluorophenyl moiety from the first fragment resulted in a secondary fragment at m/z 217. Overall, the fragmentation pattern confirmed the structure of the synthesized compound **4f**. All of the compounds were screened for *in vitro* anticancer activity. The *in silico* molecular docking and QSAR analyses were also performed to evaluate the potential target for breast cancer.

Alkaline Phosphatase Inhibitory Assay. The potential of synthesized compounds for calf intestinal phosphatase (CIAP) was evaluated. The results are summarized in Table 1. The compound **4d** showed the most potent activity with IC_{50} 1.271 μM. The compounds **4e**, **4i**, and **3f** also showed better activities with IC_{50} values of 2.943, 2.132, and 2.502, respectively. The compounds **4h**, **3d**, and **3h** showed moderate activity having IC_{50} values of 3.439, 4.768, and 4.167, respectively, while the compounds **3c**, **3e**, **3k**, **4j**, and **4f** showed low activities. The compounds **3a**, **3i**, **4c**, **4g**, and **4k** showed no inhibition.

Antioxidant Assay. Figure 2 shows the free radical scavenging activity of synthesized compounds. Among all of the compounds, the compound **4f** showed the highest percent of inhibition with an IC_{50} of 0.48 at 100 μg/mL concentration. The compounds **3e** and **4g** possessed 80% inhibition with IC_{50} values of 0.61 and 0.75 μg/mL, respectively. The compounds **3g**, **4j**, and **4h** showed approximately 70% inhibition with IC_{50} values of 1.85, 2.45, and 1.72, respectively. The compounds **3a**, **3b**, **3f**, **3h**, **3j**, and **4b** showed about 60% inhibition with IC_{50} values of 2.61, 2.6, 2.86, 2.61, 2.48, and 2.731 μg/mL at the same concentration. The compounds **3c**, **3d**, **3i**, **3k**, **4c**, **4d**, **4i**, and **4k** showed less than 50% inhibition. The standard ascorbic acid showed IC_{50} of 0.25 μg/mL at 100 μg/mL concentration.

Protein−Ligand Interaction Analysis. The protein−ligand interaction analysis was performed for the active compounds with the target protein alkaline phosphatase. The visualization of active conformation of the protein−ligand complex was done using Discovery Studio 4.0 and pymol. The protein−ligand interaction analysis showed that the compound **4d** had very stable three hydrogen bonds between the hydroxyphenyl group and ALA29, hydrogen of dihydropyrimidinone and TYR76, and oxygen of dihydropyrimidinone and HIS447. The amide−π stacked interactions were also observed between the hydroxyphenyl group and PRO28. Some π−alkyl interactions were observed with PRO75 and ALA29. The compound **4i** showed four stable hydrogen bonding of dihydropyrimidinone and GLY443 and TYR76, oxygen of dihydropyrimidinone and HIS447. The hydrogen of the hydroxyphenyl group also showed a hydrogen bond with GLU347. The $\pi-\sigma$ and alkyl interactions were observed between the hydroxyphenyl ring and ALA29 and the methoxy group with LEU26. The π−anion interactions were seen with the methoxyphenyl ring and GLU347. In compound **3f**, stable hydrogen bonding was observed between the hydrogen of the hydroxyphenyl group and THR472. The $\pi-\pi$ stacked and $\pi-\pi$ T-shaped interactions were observed between the phenyl ring of flouroaniline and TYR471, PHE464, and PHE457 and the phenyl ring of hydroxyphenyl and TYR471. π−Alkyl interactions were also observed between the phenyl ring and

Table 1. Alkaline Phosphatase Inhibitory Activity of Synthesized Compounds[a]

compound codes	alkaline phosphatase IC_{50} SEM (μM)
3a	NA[b]
3b	8.234 ± 0.265
3c	5.356 ± 0.079
3d	4.768 ± 0.149
3e	6.564 ± 0.210
3f	2.502 ± 0.023
3g	11.342 ± 0.290
3h	4.169 ± 0.154
3i	NA[b]
3j	9.436 ± 0.243
3k	6.306 ± 0.179
4a	7.678 ± 0.267
4b	8.723 ± 0.132
4c	NA[b]
4d	1.271 ± 0.0410
4e	2.943 ± 0.121
4f	6.543 ± 0.129
4g	NA[b]
4h	3.439 ± 0.139
4i	2.132 ± 0.034
4j	4.876 ± 0.086
4k	NA[b]
KH_2PO_4	2.80 ± 0.065

[a]Values are presented as mean ± standard error of mean (SEM). [b]NA - No activity.

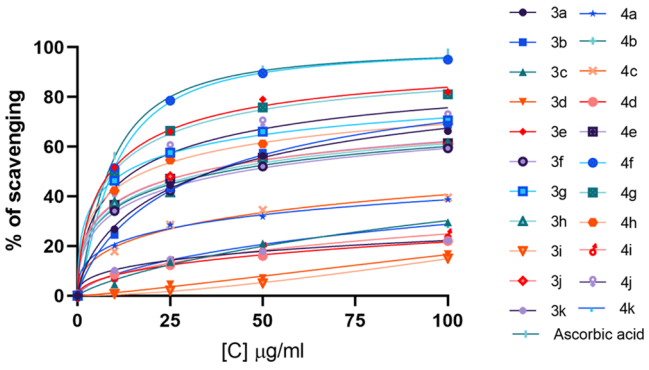

Figure 2. 2,2-Diphenyl-1-picryl-hydrazyl (DPPH) radical scavenging activity. The graph shows a linear increase in % inhibition with increasing concentration.

https://doi.org/10.1021/acsomega.1c06833
ACS Omega 2022, 7, 7139−7154

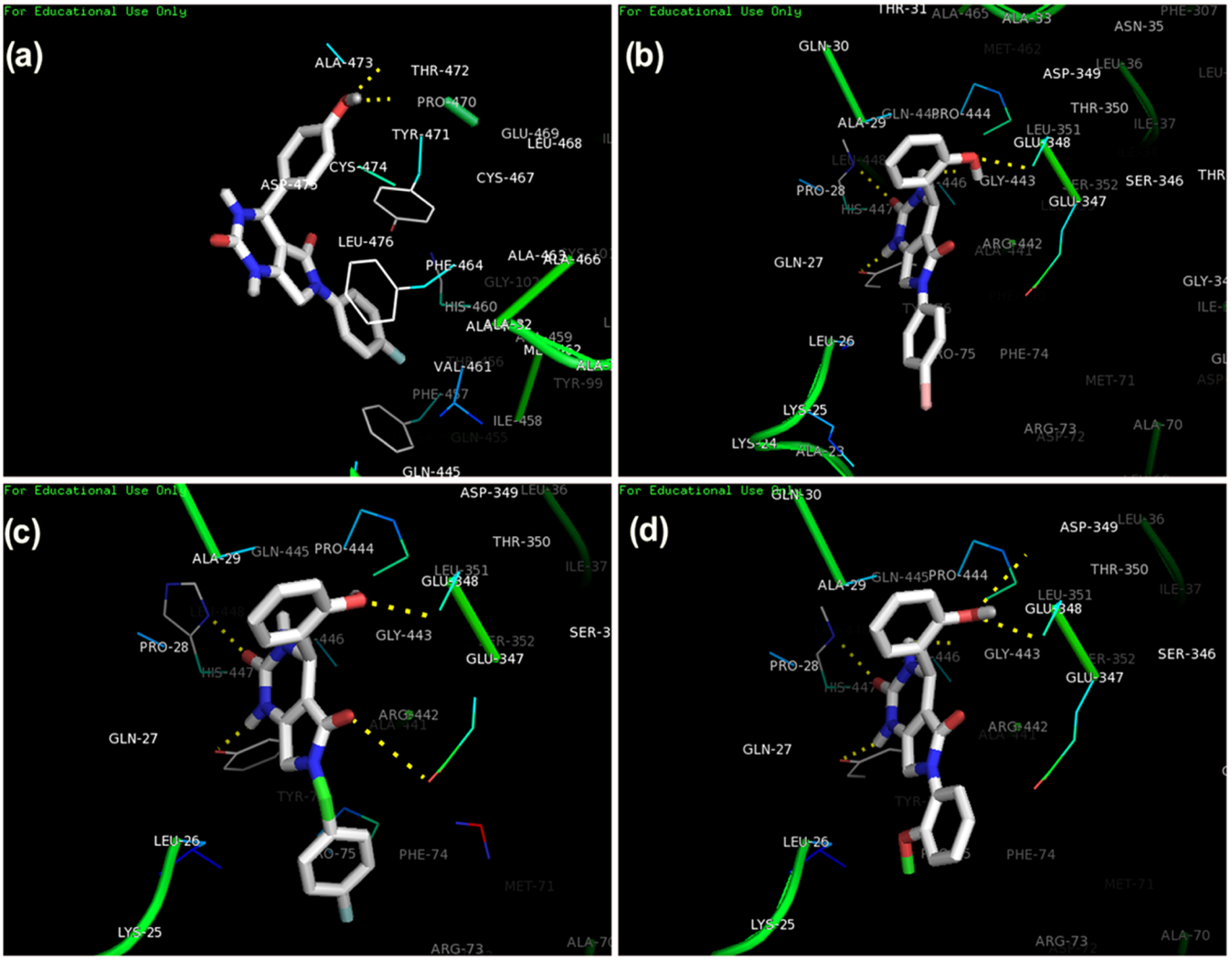

Figure 3. Binding modes of active compounds (a) **3f**, (b) **4e**, (c) **4d**, and (d) **4i** in the active binding site of alkaline phosphatase.

ALA473. However, in compound **4e**, a hydrogen bond was observed among GLU347, GLY443, HIS447, and TYR76 (Figures 3 and 4). The standard levimasole was used to compare the binding affinity and the amino acid residues involved in binding to the active site of the protein with that of active compounds. The standard levimasole showed the lowest binding affinity of −5.6 kcal/mol. The interaction analysis showed the interaction of the standard compound levimasole with the amino acid residues PHE457, PHE464, and TYR471. The oxygen atom of levimasole showed π−sulfur interaction with PHE464, while the benzene ring of levimasole showed $\pi-\pi$ stacked and $\pi-\pi$ T-stacked interaction with the amino acid PHE457 and TYR471, respectively (Figure 5).

The validation of docking was done by redocking the standard compound in the active binding site of alkaline phosphatase to ensure the docking procedure and efficiencies. The ligand was shown to bind exactly to the same active site of the protein having a root-mean-square deviation (RMSD) of −5.6 kcal/mol. The amino acid residues interacting with the ligand were PHE465, TYR471, LEU448, and VAL461 (Figure 5). The superimposition of the docked complex was done using PyMOL onto the native cocrystallized protein. A very low RMSD of 0.004 Å was observed. The superimposition of the redocked complex is shown in Figure 6. The red-color complex shows the best conformation of levimasole attained during docking, while the blue color signifies the redocked complex in the active site of the protein.

QSAR Analysis. The 22 compounds were divided into two data sets having 15 compounds as training sets and 6 compounds as test sets. PaDEL descriptor software calculated 1445 descriptors, which were further filtered using QSARINS software. The highly correlated descriptors having 90% correlation and 80% constant values were excluded from the study. The all subset method excluded 1058 descriptors from the study, and up to 8 descriptors were added to analyze the effect of descriptors on the quality of the model. Out of 20 models, one best model was selected based on the lowest lack-of-fit value. The overall performances of the models *versus* the size of the developed models were assessed by plotting the R^2 and Q_{LOO}^2 (with their standard deviation) values (Figure 7). The plot revealed an increase in the value of Q^2 and R^2 after adding the descriptors. Model 1 with five descriptors having the lowest lack-of-fit value of 0.534 was selected to calculate the alkaline phosphatase inhibitory activities. The best genetic algorithm-multiple linear regression (GA-MLR) model equation was

https://doi.org/10.1021/acsomega.1c06833
ACS Omega 2022, 7, 7139−7154

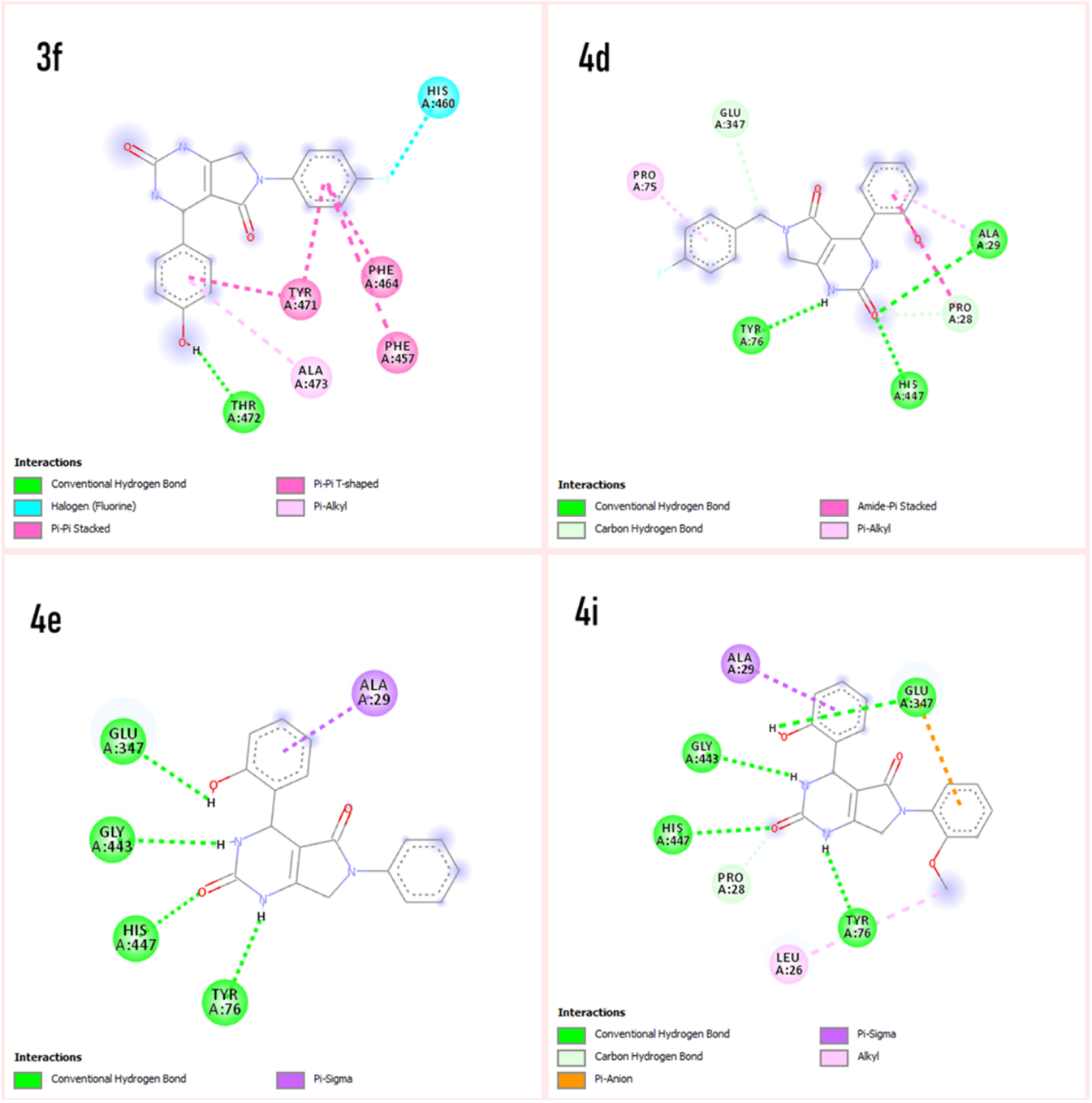

Figure 4. Interaction analysis of active compounds (**3f**, **4d**, **4e**, and **4i**) with the target protein alkaline phosphatase.

$$IC_{50} = -26.585 - 0.1570AATS5v - 85.686ATSC1c + 26.191GATS7c - 20.3112GATS3m + 0.5944minHBint8$$

The experimental IC_{50} and the predicted results by the MLR model for the training set are shown in Table 2. The Pearson correlation matrix describes the no significant multicollinearity (<0.7) among the descriptors generated and is mentioned in Table 3. The internal validation of the model, that is, the scatter plot, scatter plot by leave-one-out (LOO), scatter plot by leave-many-out (LMO), and *y*-scrambling, predicted the reliability of the model, as shown in Figure 8. William's plot and the applicability domain (AD) also defined the reliability of the model (Figure 9).

Molecular Dynamic Simulation. Using Desmond software, the molecular dynamic simulation trajectories were analyzed. The software helped in calculating the root-mean-square deviation (RMSD), root-mean-square fluctuation (RMSF) as well as the protein−ligand contacts from the MD trajectory analysis. Figure 10A displays the root-mean-square-deviation (RMSD) plots showing the complex **4d**-1EW2 reached the stable form. Larger RMSD values for the ligand than that of the protein indicate drifting away of the ligand from the initial binding site on the target protein. Figure 10B displays the local changes in the protein chain characterized by RMSF. The peaks shows the most fluctuating portion of the protein with

https://doi.org/10.1021/acsomega.1c06833
ACS Omega 2022, 7, 7139−7154

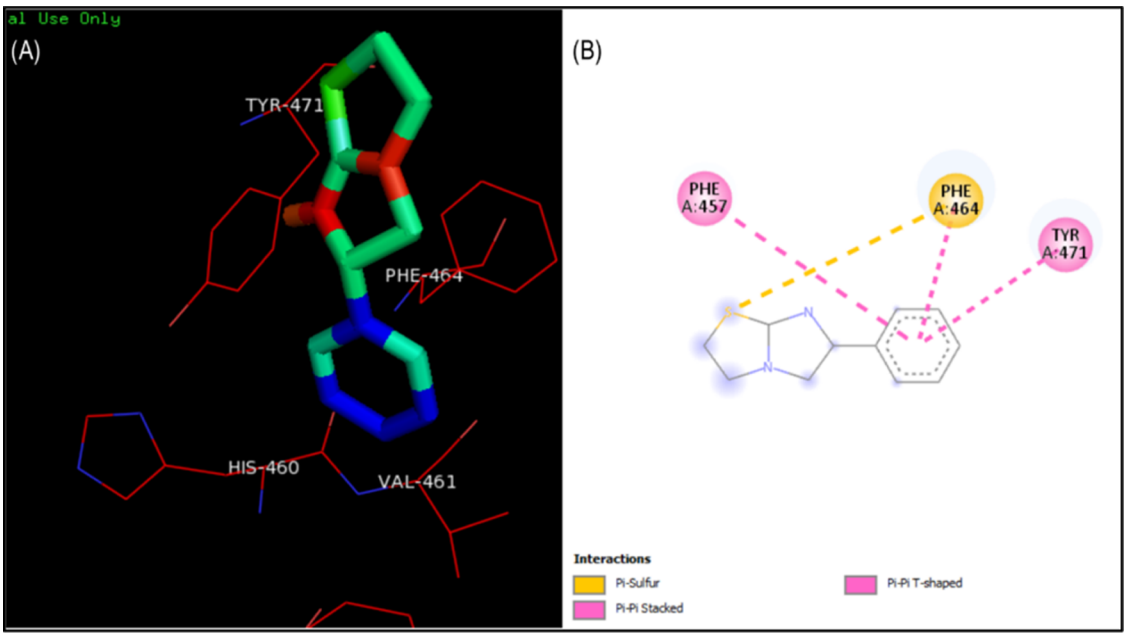

Figure 5. Binding mode and amino acid interaction of standard levimasole in the active binding site of alkaline phosphatase. (A) Surface interaction of levimasole on the active binding site of the protein. (B) 2D interaction of levimasole showing amino acid residues involved in the interaction.

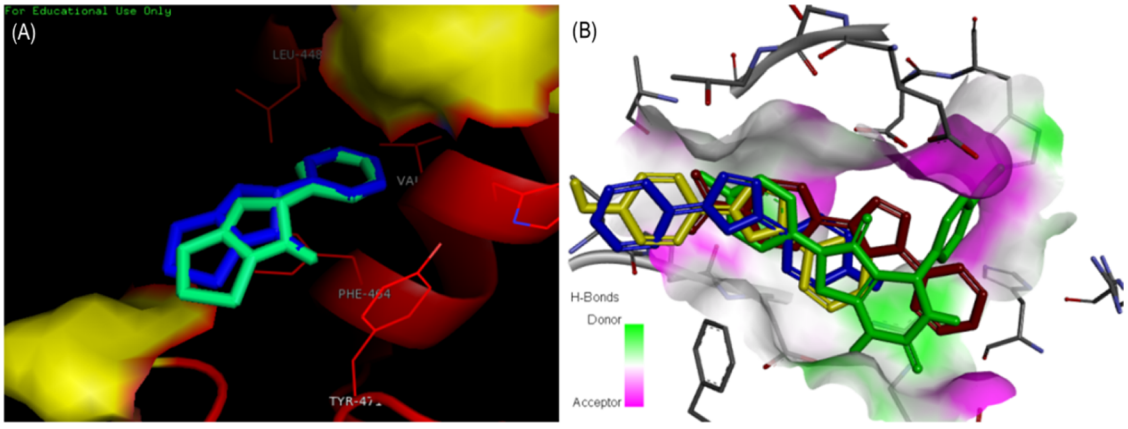

Figure 6. (A) Superimposition of the redocked complex of levimasole onto the cocrystallized complex into the active site of AP using PyMOL. (B) Superimposition of active compounds (**3f**, **4d**, **4e**, and **4i**) in the active binding site of the protein.

N terminals and C terminals being fluctuating parts on the protein. The α-helices and β-strands fluctuate less in contrast to other loop regions because of their rigid nature.

The hydrogen and hydrophobic interactions seemed to be the most significant ligand−protein interactions determined by the molecular dynamic simulations. A schematic representation of detailed ligand atom interactions with the protein residues is displayed in Figures 11 and 12. About greater than 20.0% of the interactions of the simulation time in the selected trajectory (0.00−200.20 ns) are shown. The total number of specific contacts the protein makes with the ligand is shown in the top panel of Figure 13 over the course of the trajectory. In each trajectory frame, the interaction of residues with the ligand is shown in the bottom panel. The trajectory shows more than one specific contact with the ligand for some of the residues displayed by a darker shade of orange.

DISCUSSION

Several disorders have been linked to alkaline phosphatases contributing to cancer and bone diseases. The serum levels of AP can also be used to detect multiple diseases. Hence, the alkaline phosphate inhibitory activities of synthesized dihydropyrimidinones were evaluated. The *in vitro* alkaline phosphatase inhibition assay revealed that the compounds having aromatic groups are more active than the alkyl group (**b**). Similarly, the substituted benzyl amines are more active than the substituted aromatic amines. Moreover, the −OH group at the ortho position and the electron-withdrawing group −F in compound **4d** have more potency; on replacing the group to the −para position (**3d**), the activity reduced significantly. Also, on replacing the fluorine group with chlorine (**3c**), the activity reduced significantly. The compound **4e** having the −Cl group and the ortho hydroxyl group is more active when compared to **3e** having the para hydroxyl group having a very low activity. The electron-donating group ($-OCH_3$) in **4i** at the ortho position showed good activity when compared to **3i** having the para hydroxyl group, with the activity reducing further on replacing the group from the ortho to the meta position. Compounds **3h** and **4h** having the electron-withdrawing nitro group also showed moderate activity with no significant difference in activity. The

https://doi.org/10.1021/acsomega.1c06833
ACS Omega 2022, 7, 7139−7154

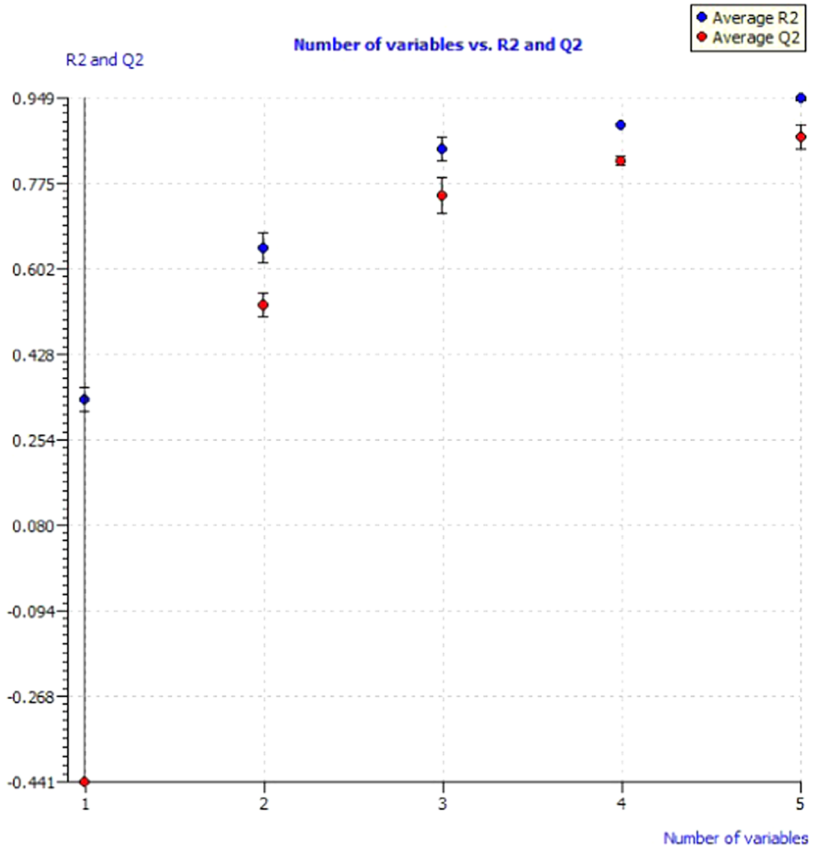

Figure 7. Model performances of different variables obtained from QSARINS.

compounds were also tested for their antioxidant activities and showed significant radical scavenging activities. The most potent activity of compound **4f** is thought to be due to the highly electronegative fluorine atom; however, by replacing the −OH group from the ortho to the para position, the activity decreased significantly to 60% in **3f**. However, in the case of **3e**, the IC_{50} was 0.61, but replacing the −OH group at the ortho position reduced the activity to 60% in **4e**, having IC_{50} 2.48. Both **3g** and **4g** showed 70−80% inhibition with IC_{50} values of 1.85 and 0.75, respectively, suggesting the effective nature of the benzimidazole group. The compounds **3h** and **4h** showed IC_{50} values of 2.61 and 1.72 μg/mL, having not much difference in inhibition, suggesting no significant effect in the change in activity by replacing the groups. The compounds having the anisidine group (**i**−**j**) showed fewer activities, with compounds **3j** and **4j** showing 60 and 70% inhibition, while **3i**, **4i**, **3k**, and **4k** showed less than 50% inhibition. The better activity of compound **4j** with IC_{50} 1.45 μg/mL may be due to the meta position of $-OCH_3$ and the ortho position of the −OH group. The compounds **3b** and **4b** showed 68 and 59% scavenging activities with IC_{50} values of 2.6 and 2.73, respectively. The compound **3a** showed IC_{50} 2.61, while **4a** showed less than 50% inhibition. The compounds **3c**, **3d**, **4c**, and **4d** showed less than 50% inhibition. The standard ascorbic acid showed IC_{50} 0.25 μg/mL with 97% inhibition (Figure 2).

QSARINS software was used to generate the model having the fitting criteria of:

N (number of compounds in the training set) = 15 R^2 (coefficient of determination) = 0.958 R_{adj}^2 (adjusted R^2) = 0.933 s (standard error of estimate) = 0.87 F (variance ratio) = 37.36.

$R^2 - R_{adj}^2$ = 0.0257, Friedman lack of fit[9] (LOF) = 5.343, k_{xx} (intercorrelation among descriptors[10]) = 0.332, ΔK (difference of correlation among the descriptors and descriptors plus the responses) = 0.029.

Root-mean-square error in fitting of the training set ($RMSE_{tr}$) = 0.360.

The coefficient of determination R^2 was found to be 0.958, closer to 1, depicting a good-quality model for inhibition of alkaline phosphatases. The low value of LOF and R_{adj}^2 of 0.933 showed no overfitting in the model and the convenience of adding a new descriptor in the model. The quality of the model can also be assessed by the presence of the least amount of descriptors, and a high F value of 37.36 and a low k_{xx} value of 0.332 showed a minimum correlation between the descriptors. The appropriate correlation between the descriptors was confirmed by the ΔK (0.029) and the small error in training sets ($RMSE_{tr}$ = 0.460; MAE_{tr} = 0.468; RSS_{tr} = 6.107; s = 0.87). The potential outliers can be seen by the scatter plot obtained by the model equation *versus* the experimental IC_{50} for training sets (Figure 8A).

Internal and External Validation of the Model. The internal validation of the model was done to check the fitting and stability of the model. The cross-validation by the leave-one-out (LOO) method showed good internal prediction as Q_{LOO}^2 = 0.903 (variance explained by LOO) has a comparable value with R^2 = 0.958. Moreover, the small error in prediction of $RMSE_{cv}$ = 1.013 and MAE_{cv} = 0.765 shows a robust and stable model. Figure 8B shows the plot between the predicted values by LOO and the experimental values of IC_{50}. The internal validation by the leave-many-out (LMO) method showed Q_{LMO}^2 = 0.690, and the calculations in each iteration of LMO and their averages are

https://doi.org/10.1021/acsomega.1c06833
ACS Omega 2022, 7, 7139−7154

Table 2. Chemical Structure and Corresponding Observed and Predicted Activities Obtained from QSARINS

Compounds	R	R'	Experimental endpoint	Predicted by model equation	Predicted model equation residual
3a	4-OH		0.00	0.65	0.65
3b	4-OH	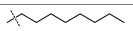	8.23	8.99	0.76
3c	4-OH	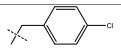	5.35	2.75	-2.59
3d	4-OH	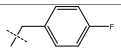	4.76	2.97	-1.78
3e	4-OH	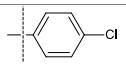	6.56	4.47	-2.08
3f	4-OH	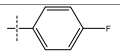	2.5	3.20	0.70
3g	4-OH	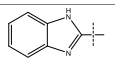	11.3	11.31	-0.02
3h	4-OH	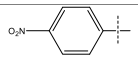	4.16	3.88	-0.27
3i	4-OH	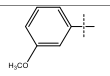	0.00	1.40	1.40
3j	4-OH	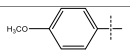	9.43	9.66	0.23
3k	4-OH		6.30	6.45	0.155
4a	2-OH		7.67	-0.39	-8.06
4b	2-OH		8.71	7.84	-0.86
4c	2-OH	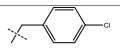	0.00	1.40	1.40
4d	2-OH	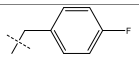	1.27	1.93	0.66
4e	2-OH	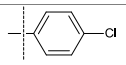	2.94	3.04	0.10
4f	2-OH	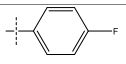	6.54	6050	-0.033
4g	2-OH	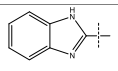	0.00	13.16	13.1
4h	2-OH	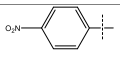	3.43	3.25	-0.17
4i	2-OH	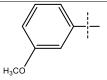	2.13	2.01	-0.11
4j	2-OH	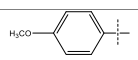	4.87	10.4	5.53
4k	2-OH		0.00	6.01	6.01

comparable to the values of R^2 and $Q_{LOO}{}^2$ of the model, revealing the stability of the model. Figure 8C displays the plot between the $Q_{LMO}{}^2$ and the correlation between descriptors and IC_{50} (k_{xy}), showing that the model is a good fit having robustness and stability. The *y*-scrambling of the model revealed a low chance of correlation as the values of R^2 and Q^2 and their averages $R_{y\text{-scr}}{}^2$

https://doi.org/10.1021/acsomega.1c06833
ACS Omega 2022, 7, 7139−7154

Table 3. Pearson Correlation Matrix

	AATS5v	ATSC1c	GATS7c	GATS3m	minHBint8
AATS5v	1.0000				
ATSC1c	−0.3123	1.0000			
GATS7c	−0.1172	0.5961	1.0000		
GATS3m	0.4945	−0.1520	0.1023	1.0000	
minHBint8	0.0467	−0.1525	−0.1751	0.1650	1.0000

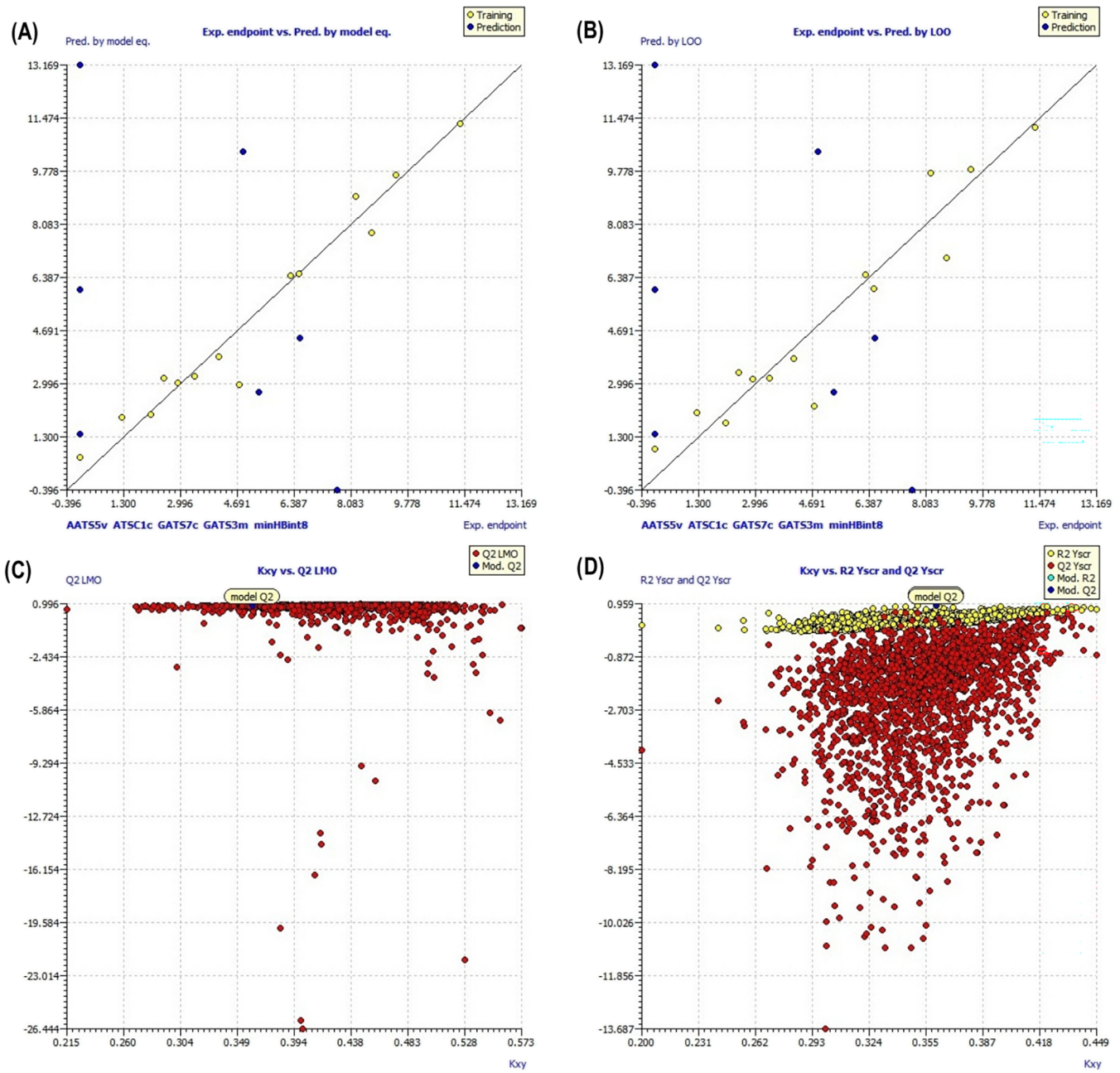

Figure 8. Internal validation of models through different methods. (A) Scatter plot of experimental IC_{50} *versus* predicted by the model equation. (B) Scatter plot obtained by the LOO method. (C) Plot comparing the original model with the LMO validations. (D) Plot comparing the original model with the *y*-scrambling model.

and $Q_{y\text{-scr}}^2$ were lower than the values obtained by previous methods. The $R_{y\text{-scr}}^2$ and $Q_{y\text{-scr}}^2$ values were 0.38 and −2.20, respectively, which are far from the values obtained for R^2 and Q^2, indicating that the model has not been obtained by random correlation. Figure 8D shows the plot between the $R_{y\text{-scr}}^2$ and $Q_{y\text{-scr}}^2$ values against the R^2 and Q^2 of the model.

The predictive ability of the model was also tested by external validation methods showing Q^2-*F*1: 0.7640; Q^2-*F*2: 0.882; Q^2-*F*3 (variances explained in external prediction[11]): 0.791; concordance correlation coeffecient[12] (CCC_{ext}): 0.9; r_m^2 aver.: 0.71; and Δr_m^2 (Roy's criteria average and Δ[13]): 0.0122. The parameters were equivalent to the values of the R^2 model. The

https://doi.org/10.1021/acsomega.1c06833
ACS Omega 2022, 7, 7139−7154

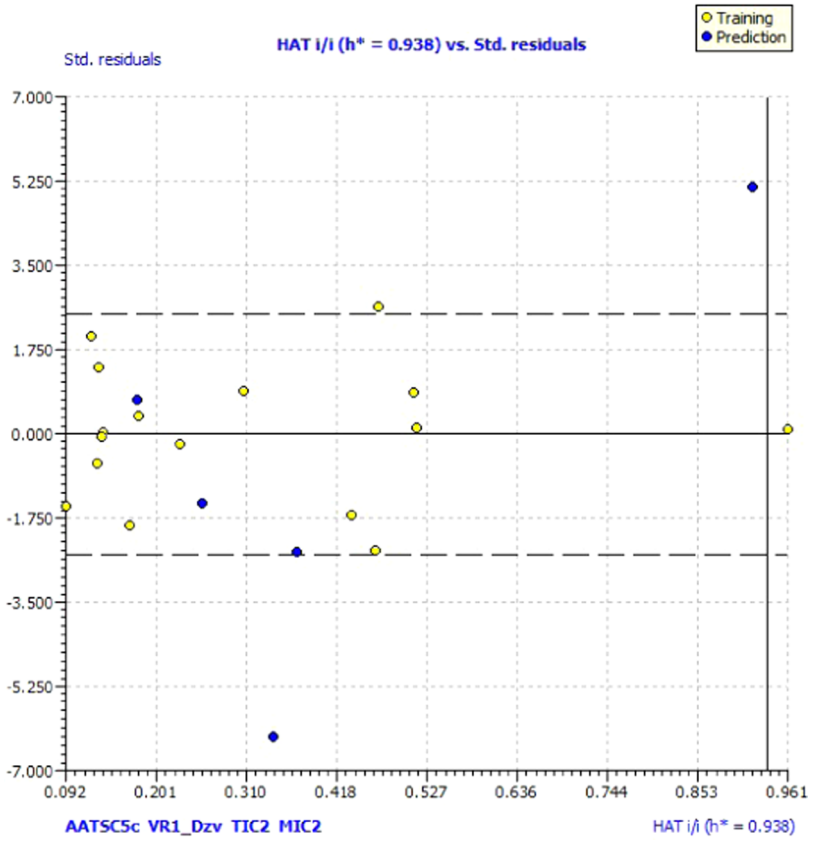

Figure 9. William's plot of the data set of IC_{50} standardized against its descriptor.

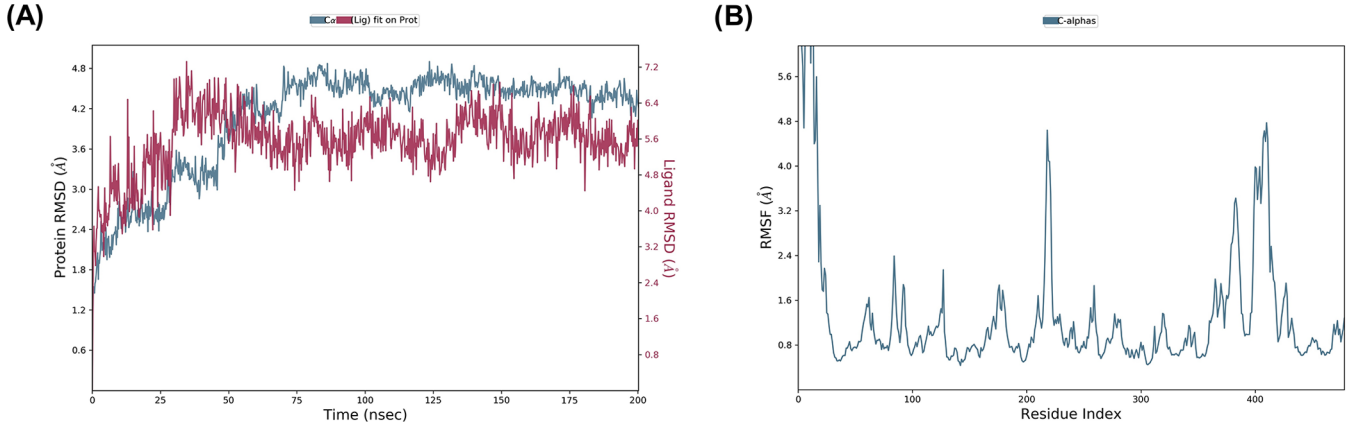

Figure 10. (A) With time, C-α atoms of the protein and ligand root-mean-square deviation (RMSD). Change in protein RMSD depicted by the left *Y*-axis over time. Change in ligand RMSD depicted by the right *Y*-axis over time. (B) Root-mean-square fluctuation (RMSF) of individual residues of the protein.

predictions of the compound in the external set are shown in Figure 8A.

The reliability of the model is detected by analyzing the number of compounds falling in the applicability domain (AD). The leverage (h) and standardized residuals were used as described by ref 14. The compounds lying in the applicability domain of the model were observed in William's graph (Figure 9) by plotting the standardized residuals for each compound against the leverage values. In the applicability domain, a leverage threshold of HAT i/i h^* = 1.000 was set up along with a defined domain constituting all of the data points within the boundary for residuals.[15] It was observed that most of the compounds fall in the applicability domain except for compounds **4a** and **4g** having values greater than the critical leverage (h = 1.29) and were considered as outliers.

Interpretation of Descriptors. The model generated by QSARINS consisted of five variables with a coefficient intercept of −26.585. The five descriptors generated were the autocorrelated descriptors AATS5v and ATSC1c (average centered Broto−Moreau's autocorrelation − lag 1/weighted by charges), GATS7c (Geary's autocorrelation − lag 7/weighted by charges), GATS3m (Geary's autocorrelation − lag 6/weighted by mass), and minHBint8.

The autocorrelated descriptors ATS5v, ATSC1c, GATS7c, and GATS3m are calculated by the Moreau−Broto (ATS) and Geary (GATS) algorithms from lag 1 to lag 8 with different

https://doi.org/10.1021/acsomega.1c06833
ACS Omega 2022, 7, 7139−7154

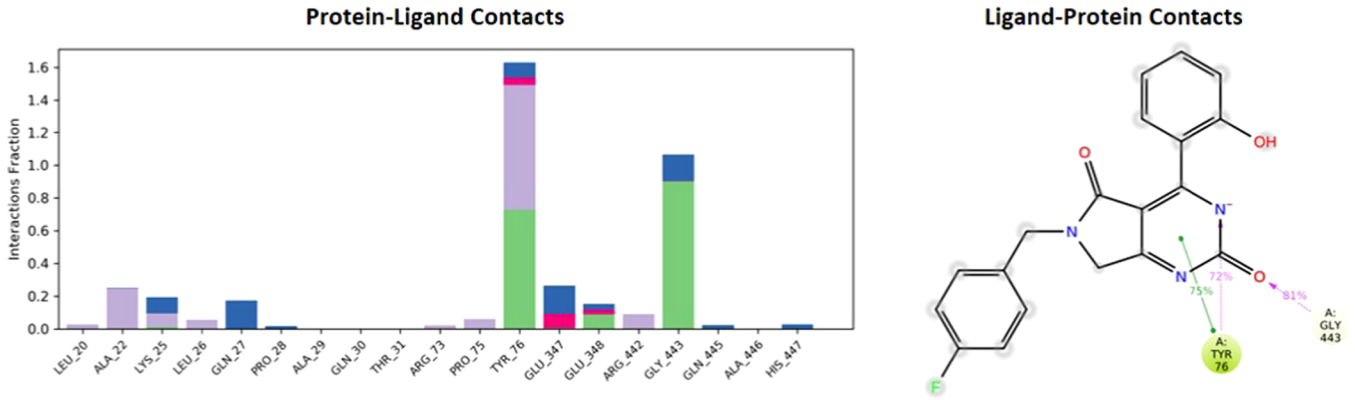

Figure 11. Protein−ligand contact histogram and ligand (**4d**) interactions of atoms with the protein residues of alkaline phosphatase.

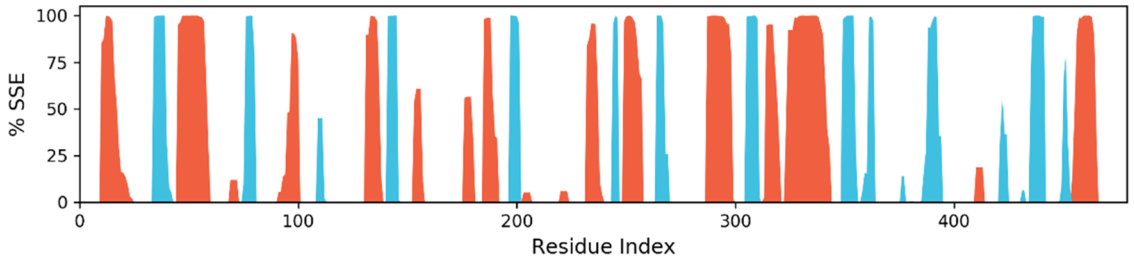

Figure 12. Representation showing the distribution of the secondary protein structure element by a residue index throughout the protein structure. The α-helices are represented by red columns, while β-strands are represented by blue columns.

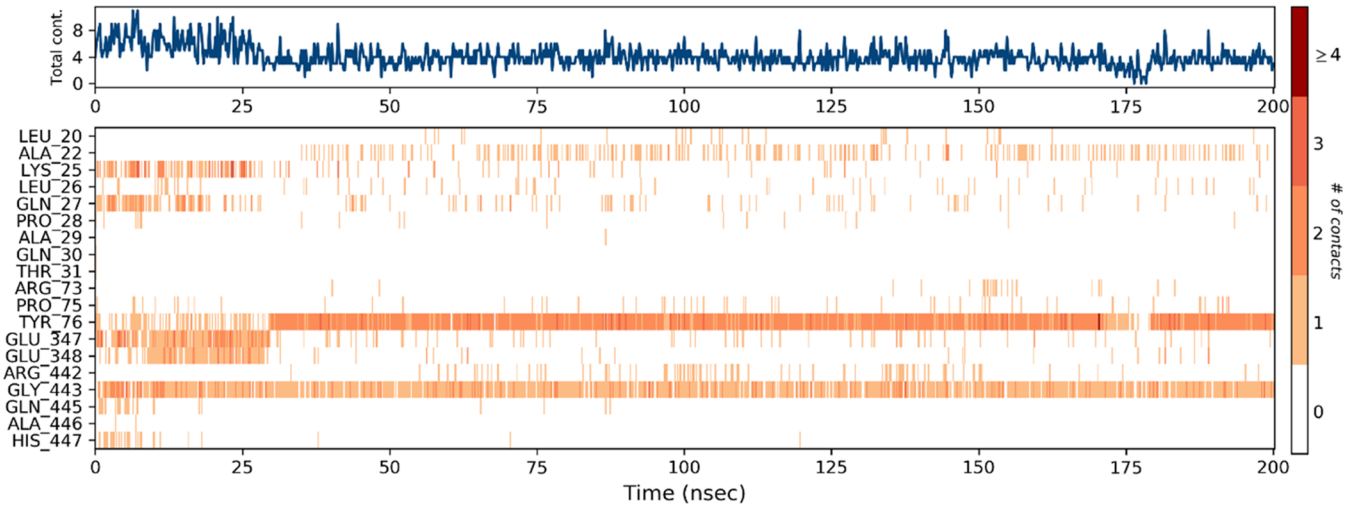

Figure 13. Timeline illustration of the protein−ligand interactions and contacts (H-bonds, ionic, hydrophobic, water bridges).

weighing patterns. These descriptors are the sum of products of atom weights of terminal atoms of all paths of the considered path length (lag). The two indices lag (d) and weight (w) are the symbols of autocorrelated descriptors, where the lag defines the topological distance between two pairs of atoms and the weight can be defined by polarizability (p), relative atomic mass (m), Sanderson's electronegativity (e), charges (c), ionization potential (i), and van der Waals volume (v). These descriptors define specific physicochemical properties associated with the topology of these structures. The GAT7c is the Geary autocorrelation descriptor of lag 7, which is weighted by charge. Similarly, GATS3m is the Geary autocorrelation descriptor of lag 3, which is weighted by the relative atomic mass. ATS5v and ATSC1c are the Moreau−Broto autocorrelation descriptors of lags 5 and 1 weighted by the van der Waals volume and charge, respectively. The AATS5v, ATSC1c, and GATS3m consist of the negative mean effect. This shows that by increasing these descriptors, there will be a decrease in the inhibitory activity. The negative coefficient is linked to enhanced binding activities of dihydropyrimidinone derivatives. The descriptor GATS7c contributed positively to the activity, suggesting that higher values would be supportive in enhancing the activity.

In the molecular simulation studies, the RMSD plot of the complex indicates that the complex reaches stability at 50 ns. From then, changes in RMSD values remain within 0.5 Å for the protein during the simulation period, which is quite acceptable. A fluctuation within 1.54 Å was observed for RMSD values of the ligand fit to the protein after gaining stability. The value indicated stable binding of the ligand to the active binding site of the protein during the simulation period (Figure 10). Keeping in

https://doi.org/10.1021/acsomega.1c06833
ACS Omega 2022, 7, 7139−7154

view the H-bonds, the amino acid TYR_76 and GLY_443 proved to be the most important residues. The normalization of the stacked bar charts was done over the course of the trajectory: for example, a value of 1.0 suggests that the particular interactions were retained for 100% of the simulation time (Figure 13). Due to multiple contacts of some protein residues of the same subtype with the ligand, values of over 1.0 are possible.

CONCLUSIONS

In this study, the inhibitory role of dihydropyrimidinone derivatives on alkaline phosphatase was studied to ascertain the possible drug targets for this enzyme. The study identified potential targets having significant alkaline phosphatase inhibitory effects that can serve as a template in drug designing. The ligand−protein binding interactions and the molecular dynamic simulations validate the molecular docking results. Among the compounds, **4d**, **4i**, **3f**, and **4e** showed potential inhibitory effects, acting as alkaline phosphatase inhibitors. Moreover, the QSAR analysis revealed the importance of autocorrelated descriptors in the structural molecule for its inhibitory activities. The investigated compounds may serve as potential pharmacophores for potent and selective alkaline phosphatase inhibitors to combat the pathological disorders due to alkaline phosphatase overexpression. We intend to further investigate the biological activities of these compounds as alkaline phosphatase inhibitors.

MATERIALS AND METHODS

Experimental Section. *Instrumentation.* The Gallenkamp (SANYO) model MPD.BM 3.5 apparatus was used to record the melting points. ^{1}H NMR spectra were measured on a Bruker AV400 spectrophotometer in CD_3OD and CD_3Cl_3 at 300 MHz with tetramethylsilane (TMS) as the internal standard. Thin-layer chromatography was used to monitor the reaction progress using silica gel HF-254-coated plates in different solvent systems with detection by UV-light absorption. The Alpha Bruker FTIR spectrophotometer (ν_{max} cm^{-1}) was used to measure the FTIR of the synthesized compounds. All of the chemicals and reagents used in the study were obtained from Aldrich Chemical Co. Mass spectral analysis was done using ionization mode MS (EI) with the JEOL 600H-1 instrument.

*General Procedure for the Synthesis of Ethyl 6-(Chloromethyl)-4-(4-hydroxyphenyl)-2-oxo-1,2,3,4-tetrahydropyrimidine-5-carboxylate (**1**).* Urea (0.01 mol), 4-chloroethylacetoacetate (0.02 mol), and 4-hydroxy benzaldehyde (0.02 mol) were refluxed for 1 h. The resulting solid was washed with water and filtered.

Yield: 53%. MP: 120 °C. R_f: 0.66. IR (ν_{max} cm^{-1}) 3408 (N−H, str); 1674 (C═O, amide, str); 755 (C−Cl, str).

*General Procedure for the Synthesis of Ethyl 6-(Chloromethyl)-4-(2-hydroxyphenyl)-2-oxo-1,2,3,4-tetrahydropyrimidine-5-carboxylate (**2**).* Urea (0.01 mol), 4-chloroethylacetoacetate (0.02 mol), and 2-hydroxy benzaldehyde (0.02 mol) were refluxed for 1 h. The resulting solid was washed with water and filtered.

Yield: 53%. MP: 190 °C. R_f: 0.66. IR (ν_{max} cm^{-1}) 3408 (N−H, str); 1674 (C═O, amide, str); 755 (C−Cl, str).

General Procedure for the Synthesis of Pyrolopyrimidines. A total of 0.001 mol of 6-chloromethyl dihydropyrimidinone was stirred in 5−10 mL of methanol, after which 0.003 mol of benzylamine was added subsequently. The mixture was first refluxed at 25 °C for 1−3 h, and then, the temperature was raised at 64 °C for 5−6 h. After completion of the reaction, the solution was cooled to ambient temperature and the solid product was filtered and washed with cold methanol to obtain the sample of desired pyrrolopyrimidines. Recrystallization was performed to obtain the analytically pure samples.

*6-Benzyl-4-(4-hydroxyphenyl)-3,4,6,7-tetrahydro-1H-pyrrolo[3,4-d]pyrimidine-2,5-dione (**3a**).* Yield: 70%. MP: ±155 °C; R_f = 0.41 (ethyl acetate/petroleum ether, 1:7); FTIR: 3590 (OH), 3455 (NH), 3100 (CH_2, sp^3), 2870 (CH, sp^3), 1690 (CO, amide), 1560 (C═C, aromatic). ^{1}H NMR (dimethyl sulfoxide (DMSO)-d_6, δ ppm): 4.10 (s, 2H), 4.33 (s, 2H), 5.10 (s, 1H), 6.65 (d, J = 8.19, Ar−2H), 7.28 (d, J = 7.7, Ar−2H), 7.29−7.34 (m, Ar−5H), 8.10−9.14 (NH, OH). ^{13}C NMR: δ = 50.1 (1C, sp^3), 52.8, 53.7 (2C, sp^3), 115−125 (4C, Ar), 128.6−128.9 (5C, Ar), 129.2 (1C, sp^2), 134.1−136.8 (2C, Ar), 137.5 (1C, sp^2), 152.4 (1C, C═O), 157.8 (1C, C−OH), 169.2 (1C, C═O). MS (EI) m/z: 335 [M].

*4-(4-Hydroxyphenyl)-6-octyl-3,4,6,7-tetrahydro-1H-pyrrolo[3,4-d]pyrimidine-2,5-dione (**3b**).* Yield: 70%. MP: ±150 °C; R_f = 0.41; FTIR: 3600 (OH), 3350 (NH), 3100 (CH, sp^2), 2870 (CH, sp^3), 1680 (CO, amide), 1560 (C═C, aromatic). ^{1}H NMR (DMSO-d_6, δ ppm): 0.86 (t, J = 7.1 Hz, J = 7.0, 3H), 1.27−3.12 (m, 14H), 4.37 (s, 2H), 5.11 (s, 1H), 6.65 (d, J = 8.19, Ar−2H), 7.28 (d, J = 7.7, Ar−2H), 8.08−9.16 (NH, OH). ^{13}C NMR: δ = 14.3−49.6 (8C, sp^3), 50.1 (1C, sp^3), 52.8 (1C, sp^3), 115−125 (4C, Ar), 129.2 (1C, sp^2), 134.8 (1C, Ar), 137.5 (1C, sp^2), 152.6 (1C, C═O), 157.8 (1C, C−OH), 169.8 (1C, C═O). MS (EI) m/z: 357 [M].

*6-(4-Chlorobenzyl)-4-(4-hydroxyphenyl)-3,4,6,7-tetrahydro-1H-pyrrolo[3,4-d]pyrimidine-2,5-dione (**3c**).* Yield: 70%. MP: ± 215 °C; R_f = 0.41; FTIR: 3650 (OH), 3490 (NH), 3100 (CH, sp^2), 2870 (CH, sp^3), 1695 (CO, amide), 1560 (C═C, aromatic). ^{1}H NMR (DMSO-d_6, δ ppm): 4.10 (s, 2H), 4.40 (s, 2H), 5.18 (s, 1H), 6.75 (d, J = 8.1, Ar−2H), 7.29 (d, J = 7.5, Ar−2H), 7.35 (d, J = 8.4, Ar−2H), 7.44 (d, J = 7.9, Ar−2H), 8.18−9.16 (NH, OH). ^{13}C NMR: δ = 50.1 (1C, sp^3), 52.8, 53.7 (2C, sp^3), 115−125 (4C, Ar), 128.3−129.9 (4C, Ar), 129.2 (1C, sp^2), 134.1−136.8 (3C, Ar), 137.5 (1C, sp^2), 152.4 (1C, C═O), 157.8 (1C, C−OH), 165.7 (1C, C═O). MS (EI) m/z: 369 [M].

*6-(4-Fluorobenzyl)-4-(4-hydroxyphenyl)-3,4,6,7-tetrahydro-1H-pyrrolo[3,4-d]pyrimidine-2,5-dione (**3d**).* Yield: 70%. MP: ± 200 °C; R_f = 0.41; FTIR: 3595 (OH), 3500 (NH), 3100 (CH, sp^2), 2870 (CH, sp^3), 1700 (CO, amide), 1560 (C═C, aromatic). ^{1}H NMR (DMSO-d_6, δ ppm): 4.19 (s, 2H), 4.30 (s, 2H), 5.19 (s, 1H), 6.64 (d, J = 7.9, Ar−2H), 7.34 (d, J = 7.7, Ar−2H), 7.11 (d, J = 7.7, Ar−2H), 7.31 (d, J = 8.3, Ar−2H), 8.8−9.10 (OH, NH). ^{13}C NMR: δ = 50.1 (1C, sp^3), 52.8, 53.7 (2C, sp^3), 112.11, 112.17 (2C, $^3J_{C-F}$ = 18 Hz), 115−125.5 (4C, Ar), 129.2 (1C, sp^2), 134.1 (1C, Ar), 139.5, 136.8 (2C, d, $^2J_{C-F}$ = 11.5 Hz), 137.5 (1C, sp^2), 137.9 (1C, Ar), 141.1, 145.9 (1C, d, $^2J_{C-F}$ = 275 Hz), 152.4 (1C, C═O), 157.8 (1C, C−OH), 168.7 (1C, C═O). MS (EI) m/z: 353 [M].

*6-(4-Chloroophenyl)-4-(4-hydroxyphenyl)-3,4,6,7-tetrahydro-1H-pyrrolo[3,4-d]pyrimidine-2,5-dione (**3e**).* Yield: 70%. MP: ±220 °C; R_f = 0.41; FTIR: 3610 (OH), 3430 (NH), 3100 (CH, sp^2), 2870 (CH, sp^3), 1680 (NH, amide), 1560 (C═C, aromatic). ^{1}H NMR (DMSO-d_6, δ ppm): 4.10 (s, 2H), 5.10 (s, 1H), 6.65 (d, J = 8.19 Hz, Ar−2H), 7.29 (d, J = 7.9 Hz, Ar−2H), 7.32 (d, J = 8.2 Hz, Ar−2H), 7.69 (s, J = 7.9 Hz, Ar−2H), 9.16 (s, NH, 1H). ^{13}C NMR: δ = 50.1 (1C, sp^3), 52.8 (1C, sp^3), 115−125 (5C, Ar), 126.2 (2C, Ar), 129.2 (1C, sp^2), 132.2−138.9

https://doi.org/10.1021/acsomega.1c06833
ACS Omega 2022, 7, 7139−7154

(4C, Ar), 137.5 (1C, sp^2), 152.4 (1C, C−O), 157.8 (1C, C−OH), 163.9 (1C, C═O). MS (EI) *m/z*: 399 [M].

6-(4-Fluorophenyl)-4-(4-hydroxyphenyl)-3,4,6,7-tetrahydro-1H-pyrrolo[3,4-d]pyrimidine-2,5-dione (***3f***). Yield: 70%. MP: ±210 °C; R_f = 0.41; FTIR: 3600 (OH), 3490 (NH), 3100 (CH, sp^2), 2870 (CH, sp^3), 1690 (CO, amide), 1560 (C═C, aromatic). ^{1}H NMR (DMSO-d_6, δ ppm): 3.9 (s, 2H), 5.15 (s, 1H), 6.7 (d, *J* = 8.0 Hz, Ar−2H), 7.29 (d, *J* = 7.9 Hz, Ar−2H), 7.05 (d, *J* = 8.1 Hz, Ar−2H), 7.60 (s, *J* = 7.9, Ar−2H), 9.06 (s, NH, 1H). ^{13}C NMR: δ = 50.1 (1C, sp^3), 52.8 (1C, sp^3), 113.23, 113.29 (2C, $^3J_{C-F}$ = 18 Hz), 115−125.5 (4C, Ar), 129.2 (1C, sp^2), 134.1 (1C, Ar), 138.3, 135.5 (2C, d, $^2J_{C-F}$ = 11.5 Hz), 137.5 (1C, sp^2), 140 (1C, Ar), 140.7, 144.7 (1C, d, J_{C-F} = 275 Hz), 152.4 (1C, C═O), 157.4 (1C, C−OH), 168.1 (1C, C═O). EIMS: *m/z* (%) = 311 (9.7, M^+ − CO), 274 (100), 263 (55), 245 (16.5), 237 (87.4), 229 (33), 219 (45), 217 (98.7), 201(68.6), 189 (20.3), 172 (14.7), 148 (29), 117 (23.5), 104 (10), 91 (15.6), 77 (12).

6-(1H-Benzo[d]imidazol-2-yl)-4-(4-hydroxyphenyl)-3,4,6,7-tetrahydro-1H-pyrrolo[3,4-d]pyrimidine-2,5-dione (***3g***). Yield: 70%. MP: ±170 °C; R_f = 0.41; FTIR: 3640 (OH), 3455 (NH), 3090 (CH, sp^2), 2870 (CH, sp^3), 1690 (CO, amide), 1585 (C═C, aromatic). ^{1}H NMR (DMSO-d_6, δ ppm): 4.09 (s, 2H), 4.90 (s, 1H), 6.78 (d, *J* = 7.19 Hz, Ar−2H), 7.48 (d, *J* = 7.3 Hz, Ar−2H), 6.93−7.4 (m, Ar−4H), 8.7−9.6 (NH, OH). ^{13}C NMR: δ = 50.1 (1C, sp^3), 52.8 (1C, sp^3), 115−125.7 (8C, Ar), 129.2 (1C, sp^2), 134.1−136.8 (3C, Ar), 137.5 (1C, sp^2), 152.4 (1C, C═O), 153.7 (1C, sp^2), 157.6 (1C, C−OH), 166.4 (1C, CO-NH). MS (EI) *m/z*: 361 [M].

6-(4-Hydroxyphenyl)-6-(2-nitrophenyl)-3,4,6,7-tetrahydro-1H-pyrrolo[3,4-d]pyrimidine-2,5-dione (***3h***). Yield: 70%. MP: ±210 °C; R_f = 0.41; FTIR: 3630 (OH), 3375 (NH), 3080 (CH, sp^2), 2900 (CH, sp^3), 1700 (CO, amide), 1490 (C═C, aromatic). ^{1}H NMR (DMSO-d_6, δ ppm): 4.10 (s, 2H), 5.10 (s, 1H), 6.65 (d, *J* = 8.19 Hz, Ar−2H), 7.28 (d, *J* = 7.9 Hz, Ar−2H), 7.6−8.1 (m, Ar−4H), 9.16 (s, NH, 1H). ^{13}C NMR: δ = 50.1 (1C, sp^3), 52.8 (1C, sp^3), 115.1−127.4 (8C, Ar), 129.2 (1C, sp^2), 133.8−140.5 (2C, Ar), 137.5 (1C, sp^2), 152.4 (1C, C−O), 157.4 (1C, C−OH), 169.8 (1C, C═O). MS (EI) *m/z*: 355 [M].

4-(4-Hydroxyphenyl)-6-(3-methoxyphenyl)-3,4,6,7-tetrahydro-1H-pyrrolo[3,4-d]pyrimidine-2,5-dione (***3i***). Yield: 70%. MP: ±190 °C; R_f = 0.41; FTIR: 3610 (OH), 3490 (NH), 3100 (CH, sp^2), 2960 (CH, sp^3), 1685 (CO, amide), 1595 (C═C, aromatic). ^{1}H NMR (DMSO-d_6, δ ppm): 3.83 (s, 3H), 4.15 (s, 2H), 5.15 (s, 1H), 6.8 (d, *J* = 7.9, Ar−2H), 7.18 (d, *J* = 7.9, Ar−2H), 6.95−7.6 (m, Ar−4H), 8−9.04 (NH, OH). ^{13}C NMR: δ = 50.1 (1C, sp^3), 52.8 (1C, sp^3), 56.0 (1C, OCH_3) 115.6−125.3 (8C, Ar), 129.2 (1C, sp^2), 133.2−134.8 (2C, Ar), 137.5 (1C, sp^2), 152.4 (1C, C═O), 157.4 (1C, C−OH), 154.9 (1C, Ar), 172.5 (1C, C═O). MS (EI) *m/z*: 351 [M].

4-(4-Hydroxyphenyl)-6-(4-methoxyphenyl)-3,4,6,7-tetrahydro-1H-pyrrolo[3,4-d]pyrimidine-2,5-dione (***3j***). Yield: 70%. MP: ±205 °C; R_f = 0.41; FTIR: 3640 (OH), 3455 (NH), 3100 (CH, sp^2), 2965 (CH, sp^3), 1690 (CO, amide), 1560 (C═C, aromatic). ^{1}H NMR (DMSO-d_6, δ ppm): 3.65 (s, 3H), 4.10 (s, 2H), 5.10 (s, 1H), 6.65 (d, *J* = 8.19 Hz, Ar−2H), 7.28 (d, *J* = 8.2 Hz, Ar−2H), 6.68 (d, *J* = 8.7Hz, Ar−2H), 7.2 (d, *J* = 8.7, Ar−2H), 8.08−9.16 (NH, OH). ^{13}C NMR: δ = 50.1 (1C, sp^3), 52.8 (1C, sp^3), 55.5 (1C, OCH_3) 114.4−125.8 (8C, Ar), 129.2 (1C, sp^2), 134.4−138.9 (2C, Ar), 137.5 (1C, sp^2), 152.4 (1C, C═O), 157.2 (1C, C−OH), 156.9 (1C, Ar), 170.6 (1C, C═O). MS (EI) *m/z*: 351 [M].

4-(4-Hydroxyphenyl)-6-(2-methoxyphenyl)-3,4,6,7-tetrahydro-1H-pyrrolo[3,4-d]pyrimidine-2,5-dione (***3k***). Yield: 87%. MP: ±215 °C; R_f = 0.41; FTIR: 3615 (OH), 3495 (NH), 3090 (CH, sp^2), 2940 (CH, sp^3), 1690 (CO, amide), 1500 (C═C, aromatic). ^{1}H NMR (DMSO-d_6, δ ppm): 3.7 (s, 3H), 4.09 (s, 2H), 5.25 (s, 1H), 6.68 (d, *J* = 8.0 Hz, Ar−2H), 7.30 (d, *J* = 7.9 Hz, Ar−2H), 6.8−7.45 (m, Ar−4H), 9.10 (s, NH, OH). ^{13}C NMR: δ = 50.1 (1C, sp^3), 52.8 (1C, sp^3), 55.5 (1C, OCH_3) 103.1−120.5 (4C, Ar), 115.1−125.8 (4C, Ar), 129.2 (1C, sp^2), 134.2−144.3 (2C, Ar), 137.5 (1C, sp^2), 152.4 (1C, C═O), 158.8 (1C, C−OH), 160.3 (1C, Ar), 163.4 (1C, CO−NH). MS (EI) *m/z*: 351 [M].

6-Benzyl-4-(2-hydroxyphenyl)-3,4,6,7-tetrahydro-1H-pyrrolo[3,4-d]pyrimidine-2,5-dione (***4a***). Yield; 87%. MP: ±195 °C; R_f = 0.41 (ethyl acetate/petroleum ether, 1:7); FTIR: 3595 (OH), 3350 (NH), 3100 (CH, sp^2), 2960 (CH, sp^3), 1695 (CO, amide), 1585 (C═C, aromatic). ^{1}H NMR (DMSO-d_6, δ ppm): 4.10 (s, 2H), 4.33 (s, 2H), 5.10 (s, 1H), 6.64−7.8 (m, Ar−9H), 8.02−9.16 (NH, OH). ^{13}C NMR: δ = 50.1 (1C, sp^3), 52.8−53.7 (2C, sp^3), 114−131.9 (10C, Ar), 129.2 (1C, sp^2), 137.1 (1C, Ar), 137.5 (1C, sp^2), 152.4 (1C, C═O), 154.6 (1C, C−OH), 172.6 (1C, C═O). MS (EI) *m/z*: 335 [M].

4-(2-Hydroxyphenyl)-6-octyl-3,4,6,7-tetrahydro-1H-pyrrolo[3,4-d]pyrimidine-2,5-dione (***4b***). Yield: 87%. MP: ±175 °C; R_f = 0.41; FTIR: 3640 (OH), 3455 (NH), 3100 (CH, sp^2), 2870 (CH, sp^3), 1660 (CO, amide), 1560 (C═C, aromatic). ^{1}H NMR (DMSO-d_6, δ ppm): 0.86 (t, *J* = 7.0, 3H), 1.27−3.12 (m, 14H), 4.11 (s, 2H), 5.10 (s, 1H), 6.64−7.3 (m, Ar−4H), 7.8−9.16 (NH, OH). ^{13}C NMR: δ = 14.3−49.6 (8C, sp^3), 50.1 (1C, sp^3), 52.8−128.9 (5C, Ar), 129.2 (1C, sp^2), 137.5 (1C, sp^2), 152.2 (1C, C═O), 154.8 (1C, C−OH), 167.5 (1C, C═O). MS (EI) *m/z*: 357 [M].

6-(4-Chlorobenzyl)-4-(2-hydroxyphenyl)-3,4,6,7-tetrahydro-1H-pyrrolo[3,4-d]pyrimidine-2,5-dione (***4c***). Yield: 87%. MP: ±220 °C; R_f = 0.41; FTIR: 3600 (OH), 3395 (NH), 3110 (CH, sp^2), 2930 (CH, sp^3), 1680 (CO, amide), 1535 (C═C, aromatic). ^{1}H NMR (DMSO-d_6, δ ppm): 4.15 (s, 2H), 4.43 (s, 2H), 5.2 (s, 1H), 6.7−7.4 (m, Ar−4H), 7.36 (d, *J* = 7.7, Ar−2H), 7.63 (s, *J* = 7.8, Ar−2H), 8.01−9.06 (NH, OH). ^{13}C NMR: δ = 50.1 (1C, sp^3), 52.8, 53.7 (2C, sp^3), 114−131.9 (9C, Ar), 129.2 (1C, sp^2), 135.5−136.8 (2C, Ar), 137.5 (1C, sp^2), 152.4 (1C, C═O), 154.6 (1C, C−OH), 169.3 (1C, C═O). MS (EI) *m/z*: 369 [M].

6-(4-Fluorobenzyl)-4-(2-hydroxyphenyl)-3,4,6,7-tetrahydro-1H-pyrrolo[3,4-d]pyrimidine-2,5-dione (***4d***). Yield: 87%. MP: ±190 °C; R_f = 0.41; FTIR: 3605 (OH), 3495 (NH), 3100 (CH, sp^2), 2900 (CH, sp^3), 1685 (CO, amide), 1560 (C═C, aromatic). ^{1}H NMR (DMSO-d_6, δ ppm): 3.9 (s, 2H), 4.29 (s, 2H), 4.90 (s, 1H), 6.73−7.5 (m, Ar−4H), 7.35 (d, *J* = 7.7, Ar−2H), 7.45 (d, *J* = 7.9, Ar−2H), 7.9−9.2 (NH, OH). ^{13}C NMR: δ = 50.4 (1C, sp^3), 52.8, 53.7 (2C, sp^3), 112.11, 112.17 (2C, $^3J_{C-F}$ = 18 Hz), 115−125.5 (4C, Ar), 129.2 (1C, sp^2), 134.1 (1C, Ar), 140.5, 137.8 (2C, d, $^2J_{C-F}$ = 11.5 Hz) 137.5 (1C, sp^2), 139.9 (1C, Ar), 142.1, 146.9 (1C, d, J_{C-F} = 275 Hz), 152.4 (1C, C═O), 154.8 (1C, C−OH), 171.7 (1C, C═O). MS (EI) *m/z* 353: [M].

6-(4-Chlorophenyl)-4-(2-hydroxyphenyl)-3,4,6,7-tetrahydro-1H-pyrrolo[3,4-d]pyrimidine-2,5-dione (***4e***). Yield: 87%. MP: ±175 °C; R_f = 0.41; FTIR: 3640 (OH), 3455 (NH), 3090 (CH, sp^2), 2890 (CH, sp^3), 1670 (CO, amide), 1600 (C═C, aromatic). ^{1}H NMR (DMSO-d_6, δ ppm): 4.12 (s, 2H), 5.10 (s, 1H), 6.7−7.35 (m, Ar−4H), 7.32 (d, *J* = 7.6, Ar−2H), 7.8 (d, *J* =

https://doi.org/10.1021/acsomega.1c06833
ACS Omega 2022, 7, 7139−7154

7.8, Ar−2H), 7.88−9.05 (NH, OH). ^{13}C NMR: δ = 50.1 (1C, sp^3), 52.8 (1C, sp^3), 114−131.9 (8C, Ar), 129.2 (1C, sp^2), 132.2−138.9 (3C, Ar), 137.5 (1C, sp^2), 152.4 (1C, C═O), 154.0 (1C, C−OH), 160.8 (1C, C═O). MS (EI) m/z = 399 [M].

6-(4-Fluorophenyl)-4-(2-hydroxyphenyl)-3,4,6,7-tetrahydro-1H-pyrrolo[3,4-d]pyrimidine-2,5-dione (***4f***). Yield: 87%. MP: ±215 °C; R_f = 0.41; FTIR: 3610 (OH), 3385 (NH), 3120 (CH, sp^2), 2910 (CH, sp^3), 1690 (CO, amide), 1515 (C═C, aromatic); ^{1}H NMR (DMSO-d_6, δ ppm): 4.20 (s, 2H), 5.20 (s, 1H), 6.64−7.3 (m, J = 8.1, Ar−4H), 7.01 (d, J = 7.7, Ar−2H), 7.6 (s, J = 7.9, Ar−2H), 7.89−9.16 (NH, OH). ^{13}C NMR: δ = 50.1 (1C, sp^3), 52.8 (1C, sp^3), 114.23, 114.29 (2C, $^3J_{C-F}$ = 18 Hz), 115−125.5 (4C, Ar), 129.2 (1C, sp^2), 134.1 (1C, Ar), 138.3, 135.5 (2C, d, $^2J_{C-F}$ = 11.5 Hz), 137.5 (1C, sp^2), 140 (1C, Ar), 140.7, 144.7 (1C, d, J_{C-F} = 275 Hz), 152.4 (1C, C═O), 154.4 (1C, C−OH), 171.1 (1C, C═O). MS (EI): m/z = 311 (9.7, M^+ − CO), 274 (100), 263 (55), 245 (16.5), 237 (87.4), 229 (33), 219 (45), 217 (98.7), 201 (68.6), 189 (20.3), 172 (14.7), 148 (29), 117 (23.5), 104 (10), 91 (15.6), 77 (12).

6-(1H-Benzo[d]imidazol-2-yl)-4-(2-hydroxyphenyl)-3,4,6,7-tetrahydro-1H-pyrrolo[3,4-d]pyrimidine-2,5-dione (***4g***). Yield: 87%. MP: ±200 °C; R_f = 0.41; FTIR: 3640 (OH), 3455 (NH), 3100 (CH, sp^2), 2870 (CH, sp^3), 1660 (CO, amide), 1560 (C═C, aromatic). ^{1}H NMR (DMSO-d_6, δ ppm): 4.05 (s, 2H), 5.05 (s, 1H), 6.7−7.5 (m, Ar−8H), 10.1 (s, NH, 1H). ^{13}C NMR: δ = 50.1 (1C, sp^3), 52.8 (1C, sp^3), 114.2−136.1 (11C, Ar), 129.2 (1C, sp^2), 137.5 (1C, sp^2), 152.4 (1C, C═O), 153.7 (1C, sp^2), 154.6 (1C, C−OH), 170.8 (1C, C═O). MS (EI) m/z: 361 [M].

4-(2-Hydroxyphenyl)-6-(2-nitrophenyl)-3,4,6,7-tetrahydro-1H-pyrrolo[3,4-d]pyrimidine-2,5-dione (***4h***). Yield: 87%. MP: ±210 °C; R_f = 0.41; FTIR: 3590 (OH), 3485 (NH), 3110 (CH, sp^2), 2900 (CH, sp^3), 1690 (CO, amide), 1545 (C═C, aromatic). ^{1}H NMR (DMSO-d_6, δ ppm): 4.10 (s, 2H), 5.10 (s, 1H), 6.66−8 (m, Ar−8H), 9.56 (NH, OH). ^{13}C NMR: δ = 50.1 (1C, sp^3), 52.8 (1C, sp^3), 114.2−133.7 (10C, Ar), 129.2 (1C, sp^2), 137.5 (1C, sp^2), 140.5 (1C, Ar), 152.4 (1C, C═O), 154.6 (1C, C−OH), 165.8 (1C, C═O). MS (EI) m/z: 355 [M].

4-(2-Hydroxyphenyl)-6-(2-methoxyphenyl)-3,4,6,7-tetrahydro-1H-pyrrolo[3,4-d]pyrimidine-2,5-dione (***4i***). Yield: 87%. MP: ±215 °C; R_f = 0.41; FTIR: 3640 (OH), 3395 (NH), 3120 (CH, sp^2), 2935 (CH, sp^3), 1695 (CO, amide), 1590 (C═C, aromatic). ^{1}H NMR (DMSO-d_6, δ ppm): 3.9 (s, 3H), 4.24 (s, 2H), 5.18 (s, 1H), 6.68−7.4 (m, Ar−8H), 9.02−10.06 (NH, OH). ^{13}C NMR: δ = 50.1 (1C, sp^3), 52.8 (1C, sp^3), 55.5 (1C, OCH_3), 114.2−133.3 (10C, Ar), 129.2 (1C, sp^2), 137.5 (1C, sp^2), 152.4 (1C, C═O), 154.6 (1C, C−OH), 154.9 (1C, Ar), 169.8 (1C, C═O). MS (EI) m/z: 351 [M].

4-(2-Hydroxyphenyl)-6-(4-methoxyphenyl)-3,4,6,7-tetrahydro-1H-pyrrolo[3,4-d]pyrimidine-2,5-dione (***4j***). Yield: 87%. MP: ±220 °C; R_f = 0.41; FTIR: 3640 (OH), 3455 (NH), 3100 (CH, sp^2), 2950 (CH, sp^3), 1680 (CO, amide), 1500 (C═C, aromatic). ^{1}H NMR (DMSO-d_6, δ ppm): 3.68 (s, 3H), 4.18 (s, 2H), 5.15 (s, 1H), 6.68−7.35 (m, 8H), 7.9−9.18 (NH, OH). ^{13}C NMR: δ = 50.1 (1C, sp^3), 52.8 (1C, sp^3), 55.5 (1C, OCH_3), 114.4−131.8 (9C, Ar), 129.2 (1C, sp^2), 138.9 (1C, Ar), 137.5 (1C, sp^2), 152.4 (1C, C═O), 154.6 (1C, C−OH), 156.9 (1C, Ar), 162.8 (1C, C═O). MS (EI) m/z: 351 [M].

4-(2-Hydroxyphenyl)-6-(3-methoxyphenyl)-3,4,6,7-tetrahydro-1H-pyrrolo[3,4-d]pyrimidine-2,5-dione (***4k***). Yield: 87%. MP: ±215 °C; R_f = 0.41; FTIR: 3625 (OH), 3475 (NH), 3110 (CH, sp^2), 2910 (CH, sp^3), 1680 (CO, amide), 1585 (C═C, aromatic). ^{1}H NMR (DMSO-d_6, δ ppm): 3.75 (s, 3H), 4.19 (s, 2H), 5.16 (s, 1H), 6.62−7.42 (m, Ar−8H), 8.01−9.26 (NH, OH). ^{13}C NMR: δ = 50.1 (1C, sp^3), 52.8 (1C, sp^3), 55.5 (1C, OCH_3), 104.1−130.5 (9C, Ar), 129.2 (1C, sp^2), 144.3 (1C, Ar), 137.5 (1C, sp^2), 152.4 (1C, C═O), 154.6 (1C, C−OH), 160.3 (1C, Ar), 172.8 (1C, C═O). MS (EI) m/z: 351 [M].

Alkaline Phosphatase Inhibition Assay. The calf intestinal alkaline phosphatase (CAIP) activity was performed according to the previously reported method using the spectrophotometric assay.[16] The inhibitory activity was measured using 50 mM Tris−HCl buffer comprising 5 mM $MgCl_2$ and 0.1 mM $ZnCl_2$ (pH 9.5). CAIP of 5 μL (0.025 U/mL) was added by preincubating the tested compounds (0.1 mM) with final DMSO 1% (v/v) and mixed for 10 min. Then, 10 μL of substrate (0.5 mM) *para*-nitrophenylphosphate disodium salt (*p*-NPP) was added to initiate the reaction and the assay mixture was incubated again for 30 min at 37 °C. A 96-well microplate reader (OptiMax, Tunable USA) was used to monitor the change in absorbance of the released *p*-nitrophenolate at 405 nm. All of the experiments were performed in triplicate by repeating. KH_2PO_4 was used as the reference inhibitor of calf ALP.

Antioxidant Activities. The 2,2-diphenyl-1-picryl-hydrazyl (DPPH) assay was used to study the free radical scavenging activity of synthesized compounds.[17] DPPH solution was prepared by dissolving 3.92 mg of DPPH in 82% methanol of 100 mL and adding it to a glass vial, making a 2800 μL DPPH solution. This was followed by the addition of 200 μL of tested compounds leading to final concentrations of 100, 50, 25, and 10 μg/mL. Mixtures were shaken well and incubated at 25 °C in the dark for 1 h. A spectrophotometer was used to measure the absorbance at 517 nm. Ascorbic acid was used as the positive control. The test was performed in triplicates, and the percentage inhibition was measured. IC_{50} values were calculated by the graphical method. The following equation was used to calculate the percent inhibition.

$$\%\ \text{scavenging effect} = \left[\frac{\text{As} - \text{Ab}}{\text{Ac}}\right] \times 100$$

where As is the absorbance of the sample, Ab is the absorbance of the blank, and Ac is the absorbance of the control.

Molecular Docking. *Preparation of the Protein.* The *in silico* protein−ligand interactions were studied to understand the binding mode of these ligands with the target protein alkaline phosphatase. The protein was retrieved from the protein data bank (www.rcsb.org) PDB ID: 1EW2. The protein was prepared before docking analysis by removing the water molecules, heteroatoms, and the cocrystallized ligands using MGL Tools-1.5.6, nonpolar hydrogen bonds were merged, AD4.2 type and Gasteiger charges were assigned, and proteins were saved in the .pdbqt format.

Preparation of the Ligand. The structures of synthesized ligands and standard Levimasole were drawn using ChemBioDrawUltra 14.0, and energy was minimized using MM2 using ChemBio3D Ultra 14.0. The structures were saved in the PDB format for AutoDock compatibility. The ligands were prepared by adding polar hydrogen atoms, the root was chosen for defining the torsion tree, and the number of rotatable bonds was identified. The ligand .pdb files were converted to the ligand.pdbqt format using MGL Tools-1.5.6 (The Scripps Research Institute).

https://doi.org/10.1021/acsomega.1c06833
ACS Omega 2022, 7, 7139−7154

AutoDock Run. The protein−ligand binding was analyzed with the help of the PyRx tool linked with AutoDock Vina to find the correct conformation and configuration of the ligands having the minimum energy structure.[18] The grid box center values (center X = 43.3, Y = 23.161, Z = 9.1269, size X = 65.56, Y = 71.79, Z = 64.64) were specified for a better conformational pattern in the active binding site of the target protein. The ligands were ranked based on the lowest binding score (kcal/mol) values. The ligand binding interaction of the best conformation was visualized using Discovery Studio 4.0 and PyMOL.

Docking Validation. The validation of the docking procedure was done by redocking the best conformation of standard levimasole to the active binding site of the protein. The same protocol was used, keeping the grid parameters unchanged. The redocking confirms the exact binding of the ligand to the active site if less deviation is observed compared to the actual complex. The redocked complex was superimposed using the Discovery studio 4.0 and PyMOL 2.3 on the reference complex. The root-mean-square deviation was calculated, and a superimposed 2D image showing amino acid residues was highlighted.

QSAR Studies. The synthesized compounds were evaluated for their structure−activity relationship for their activity against alkaline phosphatase. The models were generated using QSARINS software in accordance with the OECD standards.[19] Initially, the quantum molecular descriptors were calculated using PaDEL descriptor software linked to QSARINS. A total of 1445 descriptors were calculated. The descriptors were then imported into QSARINS software, and the highly correlated descriptors were excluded from the study.

Division of Data Sets. The data sets were divided according to the Kennard−Stone algorithm method into the training and test sets in a 4:1 ratio having 70% of the data in the training set and 30% in the test set.

QSAR Model Building. The models were built according to the all subset technique by adding descriptors one by one to see the overall effect of addition of new descriptors on the quality of the model. Up to eight descriptors were added to obtain the MLR models using the genetic algorithm (GA) technique. Twenty models were generated, and the best model was selected based on the lowest lack-of-fit (LOF) value.[20]

Validation of Models. The best model was validated by the internal and external validation methods according to the OECD principles[19] and the RMSE external, Q^2-$F1$, Q^2-$F2$, Q^2-$F3$, r_m^2, Δr_m^2, and CCC.

Cross-Validation. The cross-validation was performed by the leave-one-out (LOO) method, in which one compound is removed from the data set, while the model is calculated with the rest of the compounds. The parameters that were used to assess the quality of the model were R^2, Q_{LOO}^2, $R^2 - Q^2$, and RMSE. The leave-many-out (LMO) method was also employed for the cross-validation of the model by excluding a large number of compounds from the data set. The calculated values of R^2 and Q^2 (LMO), along with their averages that were close to R^2 and Q_{LOO}^2 values, suggested the stability of the model.

y-Scrambling. To validate whether the generated model was not due to chance correlation, the y-scrambling technique was employed. The responses were shuffled so that they were not correlated with the descriptors resulting in the poor performance of the model. The R^2 and Q^2 and their averages for y-scrambling should be less than the previously generated values for a good-quality model.

Applicability Domain. The domain of applicability was evaluated to confirm the consistency of the model within the chemical space it was developed.[21] The leverage approach was used, and William's plot was generated between the standardized residuals *versus* leverages.

Molecular Dynamic Simulation. The Desmond (2012) module of Schrodinger software was used to carry out the molecular dynamic simulation of the most active compound **4d** for 200 ns.[22] Based on the good binding score, the best conformation of **4d** was chosen for simulation studies obtained from the molecular docking studies using the OPLS-2005 force field. While the molecular docking approach provides a static view of active compounds in the active binding site of the protein, giving a prediction of the ligand binding status, the molecular dynamic simulation employs Newton's classical equation of motion by computing the atom movements over time. The physiological environment was used to carry out the simulation studies to predict the ligand binding mode. Initially, preprocessing of the ligand−protein binding complex was done using the Protein Preparation Wizard of Maestro, followed by optimization and minimization of complexes. In the orthorhombic box in a predefined TIP3P water model, the protein−ligand complex was bounded. The ions were added (Na^+ and Cl^-) to neutralize the overall charge of the system. The box volume was also minimized. The pressure and temperature were kept constant at 300 K and 1.0132 bar, and the NPT ensemble was used to perform simulations keeping in view the number of atoms, the pressure, and the time scale. The root-mean-square deviation (RMSD) was calculated for all of the trajectories to evaluate the stability of simulations.

AUTHOR INFORMATION

Corresponding Authors

Reem Altaf − *Department of Pharmaceutical Chemistry, Faculty of Pharmaceutical Sciences, Riphah International University, Islamabad 44000, Pakistan*; orcid.org/0000-0001-9398-8174; Phone: 00923175638109; Email: reemhossein@gmail.com

Syed Aun Muhammad − *Institute of Molecular Biology and Biotechnology, Bahauddin Zakariya University, Multan 60800, Pakistan*; Email: aunmuhammad78@yahoo.com

Authors

Humaira Nadeem − *Department of Pharmaceutical Chemistry, Faculty of Pharmaceutical Sciences, Riphah International University, Islamabad 44000, Pakistan*

Muhammad Nasir Iqbal − *Department of Biosciences, COMSATS University Islamabad, Sahiwal, Punjab 57000, Pakistan*

Umair Ilyas − *Department of Pharmaceutics, Faculty of Pharmaceutical Sciences, Riphah International University, Islamabad 44000, Pakistan*

Zaman Ashraf − *Department of Chemistry, Allama Iqbal Open University, Islamabad 747424, Pakistan*

Muhammad Imran − *Department of Pharmaceutical Sciences, Iqra University, Islamabad 44000, Pakistan*

Complete contact information is available at: https://pubs.acs.org/10.1021/acsomega.1c06833

Notes

The authors declare no competing financial interest.

All data generated or analyzed during this study are included in this published article.

https://doi.org/10.1021/acsomega.1c06833
ACS Omega 2022, 7, 7139−7154

REFERENCES

(1) (a) De Prada, P.; Loveland-Curtze, J.; Brenchley, J. E. Production of two extracellular alkaline phosphatases by a psychrophilic arthrobacter strain. *Appl. Environ. Microbiol.* **1996**, *62*, 3732−3738. (b) Zappa, S.; Rolland, J.-L.; Flament, D.; Gueguen, Y.; Boudrant, J.; Dietrich, J. Characterization of a highly thermostable alkaline phosphatase from the euryarchaeon *Pyrococcus abyssi*. *Appl. Environ. Microbiol.* **2001**, *67*, 4504−4511.

(2) Sharma, U.; Pal, D.; Prasad, R. Alkaline phosphatase: an overview. *Indian J. Clin. Biochem.* **2014**, *29*, 269−278.

(3) (a) Vincent, J. B.; Crowder, M. W.; Averill, B. Hydrolysis of phosphate monoesters: a biological problem with multiple chemical solutions. *Trends Biochem. Sci.* **1992**, *17*, 105−110. (b) Patel, P.; Mendall, M.; Carrington, D.; Strachan, D.; Leatham, E.; Molineaux, N.; Levy, J.; Blakeston, C.; Seymour, C.; Camm, A.; Northfield, T. C. Association of *Helicobacter pylori* and *Chlamydia pneumoniae* infections with coronary heart disease and cardiovascular risk factors. *BMJ* **1995**, *311*, 711−714.

(4) Schepeler, T.; Reinert, J. T.; Ostenfeld, M. S.; Christensen, L. L.; Silahtaroglu, A. N.; Dyrskjøt, L.; Wiuf, C.; Sørensen, F. J.; Kruhøffer, M.; Laurberg, S.; et al. Diagnostic and prognostic microRNAs in stage II colon cancer. *Cancer Res.* **2008**, *68*, 6416−6424.

(5) Lallès, J. Intestinal alkaline phosphatase: novel functions and protective effects. *Nutr. Rev.* **2014**, *72*, 82−94.

(6) (a) Ghosh, N. K.; Fishman, W. H. On the mechanism of inhibition of intestinal alkaline phosphatase by L-Phenylalanine I. Kinetic studies. *J. Biol. Chem.* **1966**, *241*, 2516−2522. (b) Hoylaerts, M.; Manes, T.; Millán, J. Molecular mechanism of uncompetitive inhibition of human placental and germ-cell alkaline phosphatase. *Biochem. J* **1992**, *286*, 23−30.

(7) Rami, C.; Patel, L.; Patel, C. N.; Parmar, J. P. Synthesis, antifungal activity, and QSAR studies of 1,6-dihydropyrimidine derivatives. *J. Pharm. Bioallied Sci.* **2013**, *5*, 277−289.

(8) (a) Snider, B. B.; Chen, J.; Patil, A. D.; Freyer, A. J. Synthesis of the tricyclic portions of batzelladines A, B and D. Revision of the stereochemistry of batzelladines A and D. *Tetrahedron Lett.* **1996**, *37*, 6977−6980. (b) Gupta, R. A.; Kaskhedikar, S. G. Synthesis, antitubercular activity, and QSAR analysis of substituted nitroaryl analogs: Chalcone, pyrazole, isoxazole, and pyrimidines. *Med. Chem. Res.* **2013**, *22*, 3863−3880. (c) Jetti, S. R.; Upadhyaya, A.; Jain, S. 3, 4-Hydropyrimidin-2-(1 H) one derivatives: solid silica-based sulfonic acid catalyzed microwave-assisted synthesis and their biological evaluation as antihypertensive and calcium channel blocking agents. *Med. Chem. Res.* **2014**, *23*, 4356−4366.

(9) Friedman, J. H. Multivariate adaptive regression splines. *Ann. Stat.* **1991**, *19*, 1−67.

(10) Todeschini, R.; Consonni, V.; Maiocchi, A. The K correlation index: theory development and its application in chemometrics. *Chemom. Intell. Lab. Syst.* **1999**, *46*, 13−29.

(11) Consonni, V.; Ballabio, D.; Todeschini, R. Comments on the definition of the Q 2 parameter for QSAR validation. *J. Chem. Inf. Model.* **2009**, *49*, 1669−1678.

(12) (a) Chirico, N.; Gramatica, P. Real external predictivity of QSAR models: how to evaluate it? Comparison of different validation criteria and proposal of using the concordance correlation coefficient. *J. Chem. Inf. Model.* **2011**, *51*, 2320−2335. (b) Chirico, N.; Gramatica, P. Real external predictivity of QSAR models. Part 2. New intercomparable thresholds for different validation criteria and the need for scatter plot inspection. *J. Chem. Inf. Model.* **2012**, *52*, 2044−2058. (c) Lawrence, I.; Lin, K. A concordance correlation coefficient to evaluate reproducibility. *Biometrics* **1989**, 255−268.

(13) Ojha, P. K.; Mitra, I.; Das, R. N.; Roy, K. Further exploring rm2 metrics for validation of QSPR models. *Chemom. Intell. Lab. Syst.* **2011**, *107*, 194−205.

(14) Atkinson, A. C. *Plots, Transformations and Regression; An Introduction to Graphical Methods of Diagnostic Regression Analysis*; Oxford University Press, 1985.

(15) Roy, K.; Kar, S.; Ambure, P. On a simple approach for determining applicability domain of QSAR models. *Chemom. Intell. Lab. Syst.* **2015**, *145*, 22−29.

(16) Iqbal, J. An enzyme immobilized microassay in capillary electrophoresis for characterization and inhibition studies of alkaline phosphatases. *Anal. Biochem.* **2011**, *414*, 226−231.

(17) Bibi, G.; Haq, I.; Ullah, N.; Mannan, A.; Mirza, B. Antitumor, cytotoxic and antioxidant potential of *Aster thomsonii* extracts. *Afr. J. Pharm. Pharmacol.* **2011**, *5*, 252−258.

(18) Dallakyan, S.; Olson, A. J. Small-Molecule Library Screening by Docking with PyRx. *Chemical Biology*; Springer, 2015; Vol. *1263*, pp 243−250.

(19) Worth, A.; Bassan, A.; De Bruijn, J.; Gallegos Saliner, A.; Netzeva, T.; Pavan, M.; Patlewicz, G.; Tsakovska, I.; Eisenreich, S. The role of the European Chemicals Bureau in promoting the regulatory use of (Q) SAR methods. *SAR QSAR Environ. Res.* **2007**, *18*, 111−125.

(20) Gramatica, P.; Chirico, N.; Papa, E.; Cassani, S.; Kovarich, S. *QSARINS: A New Software for the Development, Analysis, and Validation of QSAR MLR Models*; Wiley Online Library, 2013.

(21) Tropsha, A.; Gramatica, P.; Gombar, V. K. The importance of being earnest: validation is the absolute essential for successful application and interpretation of QSPR models. *QSAR Comb. Sci.* **2003**, *22*, 69−77.

(22) *Release, S., 1: Desmond Molecular Dynamics System*, version 3.7; D. E. Shaw Research: New York, NY, 2014. Maestro-Desmond Interoperability Tools, version, 2014, 3.

https://doi.org/10.1021/acsomega.1c06833
ACS Omega 2022, 7, 7139−7154